TECHNISCHE
UNIVERSITÄT
DARMSTADT

Institut für Kernphysik
Schloßgartenstraße 9
64289 Darmstadt, Germany

conducted at

Kyoto University

Department of Physics
Kitashirakawa-Oiwakecho
Kyoto 606-8502, Japan

Master-Thesis

Fluctuations around the Critical Point in the PNJL Model

Fluktuationen in der Nähe des kritischen Punkts im PNJL-Modell

Pascal Joachim Büscher

Supervision: Professor Jochen Wambach
Professor Teiji Kunihiro

Abstract

Susceptibilities, as well as third and fourth moments (also referred to as skewness and kurtosis, respectively), are studied in the mean-field approximation of the Polyakov-loop extended Nambu-Jona-Lasinio (PNJL) model with vector interaction.

The present study focuses on the region around the critical point of the phase diagram. The critical behavior of quadratic fluctuations is discussed by means of susceptibilities, the critical mode leading to the divergence of the susceptibilities and the Ginzburg-Levanyuk criterion which allows to examine the applicability of the employed model. Then, the third and fourth moments are evaluated in the same region and the behavior in the vicinity of the critical point is discussed. Furthermore, in order to investigate whether the calculated fourth-order could be "overshadowed" by quadratic fluctuations in experiments, the ratio of fourth moments over the squared susceptibilities is evaluated and discussed.

In addition, it is examined for all quantities how the vector interaction influences the results by varying its coupling constant.

Zusammenfassung

Suszeptibilitäten sowie dritte und vierte Momente (auch als Schiefe bzw. Kurtosis bezeichnet) werden in der Molekularfeldnäherung des um den Polyakov-Loop erweiterten Nambu-Jona-Lasinio-Modells (PNJL-Modell) mit Vektorwechselwirkung untersucht.

Diese Arbeit konzentriert sich dabei auf die Region um den kritischen Punkt im Phasendiagramm. Das kritische Verhalten von quadratischen Fluktuationen wird anhand von Suszeptibilitäten, anhand der kritischen Mode, die zur Divergenz der Suszeptibilitäten am kritischen Punkt führt, und anhand des Ginzburg-Levanyuk-Kriteriums, welches eine Untersuchung der Anwendbarkeit des verwendeten Modells erlaubt, diskutiert. Danach werden die dritten und vierten Momente in derselben Region ausgewertet und das Verhalten in der Nähe des kritischen Punkts diskutiert. Des weiteren wird das Verhältnis zwischen den vierten Momenten und dem Quadrat der Suszeptibilitäten berechnet, um zu ergründen, ob die berechneten Fluktuationen vierter Ordnung in Experimenten von Fluktuationen quadratischer Ordnung „überschattet" werden könnten.

Außerdem wird für alle Größen der Einfluss der Vektorwechselwirkung auf die Ergebnisse untersucht, indem deren Kopplungskonstante variiert wird.

Contents

1. Introduction

The comprehension of quantum chromodynamics (QCD) - the theory which describes strong interaction - and its features is an important task of modern physics. The theory is instrumental in understanding both, the early universe as well as the nature of objects in the universe in its currents form (such as neutron stars). One of the main features of QCD is "asymptotic freedom". Contrary to most fields in physics (e.g. electrodynamics), here, interactions are only small as long as only short distances are considered and become stronger for increased distances. Calculated to first order by Gross, Wilczek and Politzer in 1973 [1], the experimental confirmation of asymptotic freedom has lead to the wide acceptance of QCD as the theory describing strong interaction. Thus, in the regime of short distances, QCD can be treated perturbatively. This facilitates calculations of the structure function of hadrons among other things. However, In the present study, distances cannot be assumed to be small enough for the problem to be treated in perturbative QCD. Nevertheless, calculations in non-perturbative QCD are not feasible for most cases due to mathematical difficulties.

In theoretical physics, problems of (non-perturbative) QCD are therefore mainly approached either by (i) discretizing space-time into a finite-sized mesh ("lattice QCD") which allows for ab initio calculations or by (ii) constructing an "effective model" which shares the - for a certain problem - relevant properties with QCD while retaining a simpler mathematical structure. Nevertheless, both approaches suffer from serious limitations: Lattice QCD fails to describe QCD at finite chemical potential due to the sign problem, while effective models are only capable of reproducing QCD qualitatively. Since we are interested in properties at finite chemical potential in our study, we will employ an effective model - the so-called Polyakov-loop extended Nambu-Jona-Lasinio (PNJL) model.

The PNJL model is based on the Nambu-Jona-Lasinio (NJL) model [2], which embodies the spontaneous breaking of chiral symmetry via effective interactions between quarks (see e.g. [3–5] for reviews). Yet, it is not possible to treat confinement in such a simple model. This shortcoming is addressed in the PNJL model [6–9], where the Polyakov loop is incorporated into the model and the traced Polyakov-loop becomes an (approximate) order parameter of confinement. As for any effective model, much ambiguity is left for the choices of the interactions and their corresponding parameters. For this reason, we will vary the strength of the vector interaction in order to study its influence on our results.

A great part of the research on QCD is dedicated to the phase diagram of QCD, e.g. the diagram which maps the physically preferred phase as a function of temperature and density/chemical potential. It is known that, at low temperature and low chemical potential, the phase diagram of QCD is governed by the hadronic phase, where only bound states of two or three quarks are observed. In the realm of high temperature and/or high chemical potential, on the other hand, the phase diagram is governed by the quark gluon plasma (QGP), where quarks are not confined in bound states [10]. In addition, a color-superconducting (CSC) phase is predicted for the region of low temperature and high chemical potential [10, 11]. The transition between these phases may happen in different manner. While the order parameter defining the phases is known to change from its hadronic-phase value to its QGP-value continuously (cross-over) at high temperature and low chemical potential, a discontinuous transition (first-order phase transition) is found for high chemical potential and moderate temperature. It is still subject to speculation whether a cross-over can also be found for the transition from the hadronic phase to the CSC phase [12]. The point where the type of phase transition changes is commonly referred to as

critical point (CP). Since the CP represents an important landmark of the phase diagram, it is investigated not only in theoretical physics but also in heavy-ion collision experiments conducted at numerous research facilities worldwide as the Brookhaven National Laboratory (BNL), the European Organization for Nuclear Research (CERN) and the GSI Helmholtz Centre for Heavy Ion Research (GSI).

In order to interpret such experiments, it is crucial to know which observables are suitable probes for the critical point. For instance, it is known that susceptibilities, i.e. quadratic fluctuations with long wavelength, diverge at the CP [13] and they are thus considered possible probes for heavy-ion collision experiments [14, 15]. Although susceptibilities have been studied in the past (e.g. [16–19]), it has not been checked what influence the vector interaction has in the PNJL model. Furthermore, fluctuations of third and fourth order have been suggested as probes for the CP recently. It has been argued that they may offer better probes than susceptibilities, since (i) a change of sign in the third moments might provide additional information on the phase diagram [20] and (ii) higher-order fluctuations diverge more radically than susceptibilities at the critical point [21].

In the present study, we want to contribute to the discussion of the susceptibility as a probe for the CP and also want to address third and fourth moments. For this reason, we will employ the PNJL model mentioned above to calculate susceptibilities near the critical point and analyze the critical mode, which leads to the divergence at the CP. We will also check the quality of our model by applying the Ginzburg-Levanyuk criterion. For all these quantities, we will check how they are effected by a varied vector coupling. As for the third and fourth moments, we will investigate if the behavior predicted in [21] can also be found in the PNJL model and how it is influenced by the vector interaction. Finally, we will make predictions from our model whether there is a chance that the fourth-order fluctuations could be measured or if they are "overshadowed" by second-order fluctuations. Again, we will investigate the dependence on the strength of the vector interaction.

The present work is organized as follows: In Sec. 2, we will introduce the PNJL model and the thermodynamic relations used in the further discussion, before we will outline the phase diagram which arises from our model in Sec. 3. This provides us with the necessary devices to study quadratic fluctuations - i.e. susceptibilities, the critical mode and the Ginzburg-Levanyuk criterion - in Sec. 4 and third-order and fourth-order fluctuations in Sec. 5. In the last section, Sec. 6, we will summarize our results and will give a short outlook for future research.

2. Representation of QCD

In this section, we want to roughly outline some properties of quantum chromodynamics (QCD) before introducing the model employed in our study.

Experimental findings on the nature of nuclear matter obtained from scattering experiments have led to the development of QCD in the 1960s (cf. textbooks like [22, 23]). In QCD, the elementary particles are fermions termed quarks and their gauge bosons, which are termed gluons. There are two peculiarities of QCD which we want to highlight here: the spontaneous breaking of chiral symmetry and confinement.

Considering the spontaneous breaking of chiral symmetry from an experimental point of view, the symmetry breaking is closely connected to the pion mass. Although not completely massless, pions have a much smaller mass than other "mesons" (quark-antiquark states). Therefore, they qualify as the Nambu-Goldstone bosons of the spontaneous breaking of chiral symmetry. From the fact that the pion mass is larger than zero, it can be concluded that the symmetry has to be also explicitly broken, which accounts for by the small but finite current quark masses.

The property of confinement is closely connected to the notion of "color" charge - an additional charge apart from the electric charge, spin and parity. Due to confinement, only compounds with a total color charge of zero ("hadrons") can be detected in experiments, i.e. all observable particles are color singlets. Yet, if all quarks are close to each other, confinement is observed to play hardly any role and the particles are "asymptoticly free" [1]. If quarks were to be separated from their hadrons, the potential energy increases linearly with the distance - making it impossible to isolate quarks. Such a behavior is found to be reproduced in a non-Abelian gauge theory [25].

Especially due to the non-Abelian nature of QCD, calculations using the QCD Lagrangian are not feasible for all applications. For this reason, numerical results are usually obtained by resorting to one of the two following approximations. (i) Space-time is discretized and calculations are carried out on a finite-sized lattice ("lattice QCD") or (ii) an "effective model" is constructed which has a Lagrangian of simpler mathematical structure but shares the relevant properties with QCD. However, lattice QCD is limited to calculations with zero chemical potential μ. Results for finite chemical potential can only be gained through extrapolations and expansions around $\mu = 0$. Due to this limitation of lattice QCD, we make use of the second approach by applying the so-called Polyakov-loop extended Nambu-Jona-Lasinio (PNJL) model introduced below. It is important to notice that effective models only allow qualitative analyses, since it is not possible for an effective model to reflect all features of QCD. Hence, by choosing a certain model, one has to make compromises concerning the included features. The consequent ambiguity of effective models is illustrated in Fig. 2.1 taken from [26], where the critical points (which will be introduced in Sec. 3) of various effective models and lattice calculation are plotted as functions of chemical potential and temperature.

To get a better understanding of the model employed in the present study, its components will be analyzed. The Polyakov-loop extended Nambu-Jona-Lasinio (PNJL) model is - as the name suggests - a modification of the somewhat simpler Nambu-Jona-Lasinio (NJL) model. For this reason, this latter model will be explained first, before considering the modifications caused by the inclusion of the Polyakov loop.
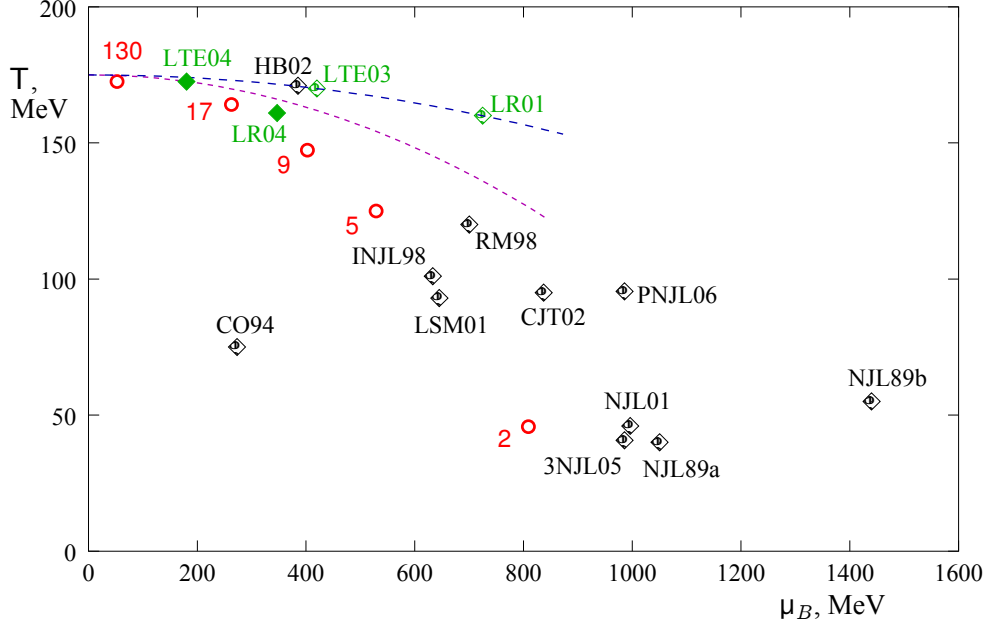
Figure 2.1: Graph taken from [26]. Critical points calculated in a variety of models. Black points represent predictions of effective models, while green points depict predictions of lattice calculations.

2.1. NJL Model

In 1961, Y. Nambu and G. Jona-Lasinio introduced a simple model which embodies the dynamical breaking of chiral symmetry [2]. They required the Lagrangian to be invariant under the following transformations of the spinor field ψ :

- $U_V(1)$ transformation

$$\psi \to e^{i\alpha}\psi, \qquad \bar{\psi} \to \bar{\psi}e^{-i\alpha}, \tag{2.1a}$$

 which guarantees particle-number conservation.

- $U_A(1)$ transformation

$$\psi \to e^{i\gamma_5\alpha'}\psi, \qquad \bar{\psi} \to \bar{\psi}e^{i\gamma_5\alpha'}, \tag{2.1b}$$

 which represents the conservation of the axial charge current.

Here, α and α' represent arbitrary phases, while γ_5 is composed of the gamma matrices through $\gamma_5 = i\gamma_0\gamma_1\gamma_2\gamma_3$. Symmetry under these two transformations is equivalent to symmetry under $U_R(1)$

$$\psi_R \to e^{i\alpha_R}\psi_R, \qquad \psi_R^\dagger \to \psi_R^\dagger e^{-i\alpha_R}, \tag{2.2a}$$

and $U_L(1)$ transformations

$$\psi_L \to e^{i\alpha_L}\psi_L, \qquad \psi_L^\dagger \to \psi_L^\dagger e^{-i\alpha_L}, \tag{2.2b}$$

where ψ_R and ψ_L denote the right- and left-handed fields $\psi_R \equiv \frac{1}{2}(1+\gamma_5)\psi$ and $\psi_L \equiv \frac{1}{2}(1-\gamma_5)\psi$, respectively. As the simplest Lagrangian that fulfills these requirements, they suggested

$$\mathcal{L}_{\text{NJL}} = \bar{\psi}i\slashed{\partial}\psi + g_0\left((\bar{\psi}\psi)^2 - (\bar{\psi}\gamma_5\psi)^2\right). \tag{2.3}$$

Apparently, the first term represents the kinetics of a Dirac spinor, while the last term represents a four-fermion interaction. After the emergence of QCD with quarks as the fermionic degrees of freedom, the original Nambu Jona-Lasinio (NJL) model was readily modified to describe interacting quarks. Translating the above equations into a three-flavor quark model (consisting of up, down and strange quarks), one requires invariance under $U_R(3) \otimes U_L(3)$ transformations

$$q_R \to e^{i\lambda \cdot \alpha_R} q_R, \qquad q_L \to e^{i\lambda \cdot \alpha_L} q_L, \tag{2.4}$$

where λ denotes the flavor-space Gell-Mann matrices and where the corresponding expressions for the hermitian conjugates have been omitted. The Lagrangian then reads [3]

$$\mathcal{L} = \overline{q} i \slashed{\partial} q + \frac{g_S}{2} \sum_{a=0}^{8} \left[(\overline{q} \lambda_a q)^2 + (\overline{q} i \gamma_5 \lambda_a q)^2 \right], \tag{2.5}$$

where the coupling constant g_S has been redefined.

However, experimental mass measurements of the pseudoscalar meson η' yielded a value that was much heavier than the pion. This finding could hardly be explained in a model retaining $U_A(1)$ symmetry, since that would require the η' to be an (approximately) massless Nambu-Goldstone boson. For this reason, in 1970, M. Kobayashi and T. Maskawa suggested a six-fermion interaction term

$$\mathcal{L}_{\det} = g_D \left(\det_{i,j} \overline{q}_i \left(1 + \gamma_5 \right) q_j + \det_{i,j} \overline{q}_i \left(1 - \gamma_5 \right) q_j \right) \tag{2.6}$$

with the determinant being taken over the flavor space as a simple way to implement this axial anomaly [27]. It is an easy task to check that this term is not conserved under transformations (2.1b). Consequently, $\mathcal{L}_{\det}$ is only invariant under $SU_R(3) \otimes SU_L(3) \otimes U_V(1)$ but not under $U_R(3) \otimes U_L(3)$ transformations. To account for the fact that chiral symmetry is also explicitly broken (see above), a current quark mass term is introduced

$$\mathcal{L}_{\mathrm{SB}} = -\overline{q} \mathbf{m} q, \qquad \mathbf{m} = \mathrm{diag}(m_{ud}, m_{ud}, m_s), \tag{2.7}$$

where $m_u = m_d = m_{ud}$ accounts for isospin symmetry. It should be noted that this term explicitly breaks the chiral symmetry $SU_R(3) \otimes SU_L(3)$, but that this is only a "soft" symmetry breaking as long as only small quark masses are applied.

The symmetries presented above also allow for further interactions to be included - even on the level of four-fermion interactions. In this work, we want to discuss the vector-vector interaction. For simplicity, we assume the vector channel to be independent of flavor and include it by supplementing the Lagrangian with

$$\mathcal{L}_{\mathrm{V}} = -g_V (\overline{q} \gamma_\mu q)^2. \tag{2.8}$$

NJL models of this kind have been studied thoroughly in the past and are reviewed, for instance in [3–5].

2.1.1. Mean-Field Approximation

The mean-field approximation (MFA), which is also reviewed in [3–5], presents us with a approximation that simplifies calculations drastically. In this approximation, it is assumed that, for all quantities A, fluctuations - i.e. deviations from the thermal average $\langle A \rangle$ - are small. Thus,

expanding the Lagrangian to first order in $\overline{q}\Gamma q$ around $\langle\overline{q}\Gamma q\rangle$ (where $\Gamma = 1, \gamma_5, \gamma_\mu, \gamma_\mu\gamma_5$) yields the expressions in the MFA. Then, the four-fermion interactions are approximated by

$$(\overline{q}\Gamma q)^2 \approx \langle\overline{q}\Gamma q\rangle^2 + 2\left(\overline{q}\Gamma q - \langle\overline{q}\Gamma q\rangle\right)\langle\overline{q}\Gamma q\rangle = 2\overline{q}\Gamma q \langle\overline{q}\Gamma q\rangle - \langle\overline{q}\Gamma q\rangle^2, \tag{2.9a}$$

while the six-fermion interaction becomes

$$\begin{aligned}
Q_1 Q_2 Q_3 &\approx \langle Q_1\rangle\langle Q_2\rangle\langle Q_2\rangle + ((Q_1 - \langle Q_1\rangle)\langle Q_2\rangle\langle Q_3\rangle + \text{ cyclic permut. }) \\
&= (Q_1\langle Q_2\rangle\langle Q_3\rangle + \text{ cyclic permut. }) - 2\langle Q_1\rangle\langle Q_2\rangle\langle Q_2\rangle.
\end{aligned} \tag{2.9b}$$

with $Q_{1\ldots3}$ being $\overline{q}_i q_j$ or $\overline{q}_i\gamma_5 q_j$ with arbitrary i, j. The only expectation values considered to have non-vanishing values are the chiral condensates $\sigma_i \equiv \langle\overline{q}_i q_i\rangle$ (with $i = u, d, s$) and the quark number density $\rho \equiv \langle\overline{q}\gamma_0 q\rangle$. The condensates $\langle\overline{q}_i q_j\rangle$ with $i \neq j$ vanishes since it is assumed that flavor is conserved. To be exact, the condensates $\langle\overline{q}_i\gamma_5 q_j\rangle$, which corresponds e.g. to pions, should be assigned with variables. Yet, by employing the gap equations, which will be introduced in the next subsection, to determine the equilibrium state, it turns out that the pion condensates vanish for any μ, T as long as the ground state is required to be homogeneous. Consequently, they can be neglected from the beginning. Summarizing the above discussion, we arrive at the Lagrangian

$$\mathcal{L} = \overline{q}\left(i\slashed{\partial} + 2g_V\gamma_0\rho - \mathbf{M}\right)q - g_S\left(2\sigma_u^2 + \sigma_s^2\right) + g_V\rho^2 - 4g_D\sigma_u^2\sigma_s, \tag{2.10}$$

where $\mathbf{M} = \text{diag}(M_u, M_u, M_s)$ with the constituent quark masses

$$\begin{aligned}
M_u &= m_{u,d} - 2g_S\sigma_u - 2g_D\sigma_u\sigma_s, \\
M_s &= m_s - 2g_S\sigma_s - 2g_D\sigma_u^2.
\end{aligned} \tag{2.11}$$

Here, we have introduced only two different chiral condensates, since isospin symmetry is assumed to be conserved and thus $\sigma_u = \sigma_d$. The question whether the MFA is a good approximation for our applications will be addressed in Sec. 4.1.2.

2.1.2. Thermodynamic Potential

For the calculations in the present study, it is necessary to recall some relations from statistical physics and finite-temperature quantum field theory (cf. [23]). First, we start with the grand canonical partition function

$$Z \equiv \text{Tr } e^{-\beta(H-\mu\hat{N})} = \sum_a \int \mathrm{d}\Psi_a \langle\Psi_a| e^{-\beta(H-\mu\hat{N})} |\Psi_a\rangle \tag{2.12}$$

with $\beta \equiv T^{-1}$, the chemical potential μ and the quark number operator $\hat{N}$. The sum $\sum_a \int \mathrm{d}\Psi_a$ is carried out over all states Ψ_a. From the obvious analogy to the (real-time) transition amplitude $\langle\Psi_a| e^{-iHt} |\Psi_a\rangle$, it is found that after a transformation to imaginary time $\tau = it$

$$Z = \int \mathcal{D}iq^\dagger\mathcal{D}q \exp\left[\int_0^\beta \mathrm{d}\tau \int \mathrm{d}^3x \left(\mathcal{L} - \mu\overline{q}\gamma_0 q\right)\right], \tag{2.13}$$

where the functional integral $\int \mathcal{D}iq^\dagger\mathcal{D}q$ covers all quark species. The grand canonical potential can now be employed to define the effective potential

$$\Omega \equiv -T\ln Z. \tag{2.14}$$

Before we can calculate numerical values of Ω for the mean-field NJL Lagrangian (2.10), we have to solve the functional integrals in (2.13). While the terms independent of q, $\overline{q}$ can be factorized in Z and become simple summands in Ω, the first term of (2.10) can be taken care of by applying

$$\ln \left(\int \mathcal{D}iq^\dagger \mathcal{D}q e^{iq^\dagger A q} \right) = \ln \det A = \text{Tr} \ln A. \tag{2.15}$$

In our case, a Fourier transformation of (2.13) leads to $A = -i\beta \left((-i\omega_n + \mu - 2g_V \rho) - \gamma_0 \vec{\gamma} \vec{p} - \gamma_0 \text{M} \right)$. The so-called Matsubara frequency ω_n is the transform of τ and one finds that $\omega_n = (2n+1)\pi T$, since the relevant $q(\vec{x}, \tau)$ have to fulfill the condition $q(\vec{x}, 0) = -q(\vec{x}, \beta)$ as a consequence of the trace operation and the antisymmetry condition of fermions. The sum over the Matsubara frequencies is solved by converting the sum $T \sum_{\omega_n} f(i\omega_n)$ into an integral of the function $\frac{1}{4\pi i} f(p_0) \tanh \left(\frac{1}{2} \beta p_0 \right)$ over p_0 with a closed integration path which includes all ω_n. Then, the integral can be solved by changing the integration path. This yields

$$\Omega_{\text{NJL}}/V = -2N_c \sum_{i=u,d,s} \int \frac{\text{d}^3 p}{(2\pi)^3} \left(E_i(p) + T\ln\left(1 + e^{-\beta(E_i(p)-\tilde{\mu})} \right) + T\ln\left(1 + e^{-\beta(E_i(p)+\tilde{\mu})} \right) \right)$$
$$+ g_S \left(2\sigma_u^2 + \sigma_s^2 \right) - g_V \rho^2 + 4g_D \sigma_u^2 \sigma_s, \tag{2.16}$$

where the factor of $2N_c$ is due to the degeneracy in spin and color, the energy $E_i(p)$ is given by $E_i(p) = \sqrt{p^2 + M_i^2}$ and $\tilde{\mu}$ is defined by $\tilde{\mu} \equiv \mu - 2g_V \rho$. Note that the integral over the zero-point energy - the first term in the momentum integral - diverges. This problem is circumvented by simply applying an ultraviolet cutoff Λ to the integral. This is legitimate, since the parameters of an effective model are fixed such that it reproduces certain physical results which are known from experiment (cf. Sec. 2.1.3). Owing to this fixing of the parameters, an effective model is limited to the energy scale on which the parameters were determined. Hence, there is no problem in cutting of the momentum integral, as long as the integral is guaranteed to include the relevant energy scale. To simplify numerical calculations, we apply the cutoff to the whole integral instead of applying it solely to the zero-point energy. It also should be noted that only the second and third terms in the momentum integral depend on T and μ and become 0 for $T = \mu = 0$. They apparently obey the Fermi-Dirac statistics of fermions and represent the thermal energy of quarks (second term) and antiquarks (third term). The various interactions are contained not only in the second line of (2.16), but also in the first line of the same equation through E_i and $\tilde{\mu}$.

From thermodynamics it is known that the equilibrium state (for fixed T, μ) is given by the chiral condensates that minimize Ω_{NJL}. Apparently, they have to fulfill the (necessary) stationary condition

$$\frac{\partial \Omega_{\text{NJL}}}{\partial \langle \rangle_i} = 0 \quad \text{for } \langle \rangle_i = \sigma_u, \sigma_s. \tag{2.17}$$

The quark-number density ρ can be gained from the well-known thermodynamic relation

$$\rho = -\frac{\partial(\Omega/V)}{\partial \mu}, \tag{2.18}$$

which is apparent, if the way how the chemical potential was included into the model is considered. It should be noted that the last equation is equivalent to condition

$$\frac{\partial \Omega_{\text{NJL}}}{\partial \rho} = 0 \tag{2.19}$$
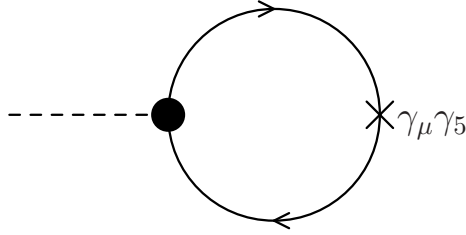
Figure 2.2: Feynman diagram used for the calculation of the pion decay constant f_π. The dashed line denotes a pion, while the continuous ones denote quarks.

for $g_V \neq 0$. The equations (2.17) and (2.19) are commonly referred to as the gap equations. When employing the gap equations to determine the equilibrium, one has to keep in mind that there may be more than one combination of condensates that solve these equations. In a numerical calculation, the rootfinding procedure, therefore, has to be repeated for several starting values to make sure all minima are obtained. From all obtained minima, the one with lowest Ω is chosen.

2.1.3. Model Parameters

In the above discussion, we have reviewed the tools necessary to calculate the equilibrium state of our NJL model for given temperature T and chemical potential μ. However, in order to carry out numerical calculations, numerical values need to be assigned to parameters in the model. These parameters are the coupling constants g_S, g_D, g_V, the quark masses m_{ud}, m_s and the three-momentum cutoff Λ.

We adopt the parameters from [3], where the parameters are fixed for a NJL model containing the scalar and the determinant but not the vector interaction. We summarize the procedure that provided the authors of [3] with their parameter set. First, it is assumed that $m_{u,d} = 5.5\,\text{MeV}$, which is argued to be well consistent with the range of $5\dots9\,\text{MeV}$, that has been manifested for m_{ud} at an energy scale of $1\,\text{GeV}$ by investigating meson and baryon spectra, QCD sum rules and other means. The other parameters are then determined such that they reproduce the experimental values

$$m_\pi = 138\,\text{MeV}, \quad f_\pi = 93\,\text{MeV}, \quad m_K = 495.7\,\text{MeV}, \quad m_{\eta'} = 957.5\,\text{MeV} \qquad (2.20)$$

at $T, \mu = 0$, where m_π, m_K and $m_{\eta'}$ are the masses of the pion, the kaon and the η' meson, while f_π denotes the decay constant of the pion. For given test values, the meson masses are obtained from the poles of the meson propagator in the random-phase approximation (RPA). For the η', one has to take care of the coupling to the η. The decay constant f_π on the other hand is gained by evaluating the loop diagram displayed in Fig. 2.2. This leads to the parameter set

$$\Lambda = 631.4\,\text{MeV}, \quad m_s = 135.7\,\text{MeV}, \quad g_s = 3.67\Lambda^{-2}, \quad g_D = -9.29\Lambda^{-5}. \qquad (2.21)$$

It should be noted that the values which were used to fit the model parameters are those considered valid at the time [3] was written. Nowadays, slightly different values are anticipated [28]. For instance, the light quark mass is assumed to be within in a range of $2.5\dots5\,\text{MeV}$, while $m_s = 105^{+25}_{-35}\,\text{MeV}$ is assumed for the strange quark mass. Considering the uncertainties of these values, we adopt the model parameters from [3], since they do not differ much from the "old" values.

The fact that the vector interaction is not included here is not important, since ρ turns out to be 0 at zero chemical potential and the vector interaction does thus have no influence here. There are studies, e.g. in the instanton-antiinstanton molecule model [29], which predict g_V to be of the order $g_S/4$. Since we are interested in the influence of the vector interaction, we do not assign a fixed value to g_V here and will vary it as a free parameter.

2.2. PNJL Model

Although the NJL model introduced above has proved to be a very handy device to better understand QCD, it fails to describe effects involving confinement. The Polyakov-loop extended Nambu-Jona-Lasinio (PNJL) model aims to overcome this caveat by supplementing the NJL model with additional order parameters describing confinement - the (traced) Polyakov loop [6].

2.2.1. Polyakov Loop

The Polyakov loop [30] has its origin in lattice gauge theory. There, in contrast to the NJL model, the focus is put on the dynamics of gluons (the gauge bosons of QCD), while, in pure lattice gauge theory, the dynamics of quarks is even neglected. The symmetry connected to confinement (being obeyed in the confined phase and being broken in the deconfined phase) is the center symmetry $Z(3)$. The center symmetry can be expressed in the language of lattice gauge theory as the symmetry under the transformation of the temporal link variable $U_4(\tau = N_\tau) \to zU_4(\tau = N_\tau)$ with $zz^\dagger = z^3 = 1$ [31]. Apparently, the condition $zz^\dagger = 1$ allows for meson states to exist, while the condition $z^3 = 1$ gives rise to the existence of baryon states. This symmetry also applies to the Polyakov loop L which is defined as [6]

$$L(\vec{x}) = \mathcal{P} \exp\left[i \int_0^\beta \mathrm{d}\tau A_4(\vec{x}, \tau)\right]. \tag{2.22}$$

Note that L is a matrix in color space. We have denoted the path ordering with $\mathcal{P}$ and the temporal component of the gauge field with A_4. The spatial components are assumed to have no contribution. If this equation was to be expressed in lattice gauge theory, one would obtain a sum of link variables.

In the PNJL model, the Polyakov loop contributes to the thermodynamic potential in two ways: (i) through an effective potential depending on the Polyakov loop and the temperature and (ii) through a coupling between the quarks and the Polyakov loop. The Polyakov-loop potential has to be chosen such that the center symmetry is broken only dynamically. Consequently, it should consist only of $LL^\dagger$, L^3, $L^{\dagger 3}$, T and constant factors. These conditions allow to construct an ansatz that is fitted to data from lattice gauge theory. In this work, we adopt the logarithmic potential

$$\Omega_{\mathrm{pol}}(\ell, \bar{\ell}, T) = -0.03\Lambda^3 VT \left(54\mathrm{e}^{-664\,\mathrm{MeV}/T}\ell\bar{\ell} + \ln\left[1 - 6\ell\bar{\ell} - 3(\ell\bar{\ell})^2 + 4(\ell^3 + \bar{\ell}^3)\right]\right) \tag{2.23}$$

from [7]. ℓ and $\bar{\ell}$ denote the traced Polyakov loop given by

$$\ell \equiv \frac{1}{N_c} \langle \mathrm{Tr}_c L\rangle, \qquad \bar{\ell} \equiv \frac{1}{N_c} \left\langle \mathrm{Tr}_c L^\dagger\right\rangle, \tag{2.24}$$

where the trace Tr_c only runs over color space. The choice of the potential, however, is not unambiguous. [6] and [8], for instance, construct PNJL models employing other potentials. The

coupling to quarks can be elucidated by recalling that the gauge field couples to the quarks in the QCD Lagrangian through $-\overline{q}i\slashed{A}q$ (Note, that the coupling constant and the Gell-Mann matrices usually apparent in QCD have been absorbed into A_μ here). The coupling to quarks is thus equivalent to an imaginary quark chemical potential. Employing the Polyakov loop, one finds that the thermal energy of quarks and antiquarks in (2.16) turns into

$$-2T \sum_{i=u,d,s} \int \frac{\mathrm{d}^3 p}{(2\pi)^3} \left(\ln \det_c \left[1 + L e^{-\beta(E_i(p)-\tilde{\mu})} \right] + \ln \det_c \left[1 + L^\dagger e^{-\beta(E_i(p)+\tilde{\mu})} \right] \right) \qquad (2.25)$$

with the determinant over color space $\det_c$. It should be noted that, due to this term, center symmetry is explicitly broken in the PNJL Lagrangian. Consequently, the Polyakov loop is no longer a well-defined order parameter. This fact leads to a smoothening of the phase transition of confinement for calculations employing the PNJL model (as it does for comparable lattice calculations) [9].

Taking the thermal average over the determinants in (2.25) yields [7]

$$
\begin{aligned}
\left\langle \det_c \left[1 + L e^{-\beta(E_i(p)-\tilde{\mu})} \right] \right\rangle &= 1 + e^{-3\beta(E_i(p)-\tilde{\mu})} + 3\ell e^{-\beta(E_i(p)-\tilde{\mu})} + 3\bar{\ell} e^{-2\beta(E_i(p)-\tilde{\mu})}, \\
\left\langle \det_c \left[1 + L^\dagger e^{-\beta(E_i(p)+\tilde{\mu})} \right] \right\rangle &= 1 + e^{-3\beta(E_i(p)+\tilde{\mu})} + 3\bar{\ell} e^{-\beta(E_i(p)+\tilde{\mu})} + 3\ell e^{-2\beta(E_i(p)+\tilde{\mu})}.
\end{aligned}
\qquad (2.26)
$$

This average is employed as the mean-field expression for the thermal energy and we arrive at the thermodynamic potential of our PNJL model

$$
\begin{aligned}
\frac{\Omega_{\mathrm{PNJL}}}{V} = &-2 \sum_{i=u,d,s} \int_0^\Lambda \frac{\mathrm{d}^3 p}{(2\pi)^3} \left(3E_i(p) + T \ln \left(1 + e^{-3\beta(E_i(p)-\tilde{\mu})} + 3\ell e^{-\beta(E_i(p)-\tilde{\mu})} + 3\bar{\ell} e^{-2\beta(E_i(p)-\tilde{\mu})} \right) \right. \\
&\left. + T \ln \left(1 + e^{-3\beta(E_i(p)+\tilde{\mu})} + 3\bar{\ell} e^{-\beta(E_i(p)+\tilde{\mu})} + 3\ell e^{-2\beta(E_i(p)+\tilde{\mu})} \right) \right) \\
&+ g_S \left(\sigma_u^2 + \sigma_d^2 + \sigma_s^2 \right) - g_V \rho^2 + 4g_D \sigma_u \sigma_d \sigma_s + \Omega_{\mathrm{pol}}(\ell, \bar{\ell}, T)/V.
\end{aligned}
\qquad (2.27)
$$

From this expression, it is obvious that at $\mu = 0$ - which is, as mentioned above, equivalent to $\tilde{\mu} = 0$ - (2.27) is symmetric to $\ell \leftrightarrow \bar{\ell}$ and consequently $\ell = \bar{\ell}$ due to the gap equations. Furthermore, it is an easy task to check that $\ell, \bar{\ell} \to 0$ for $T \to 0$ and that $\ell, \bar{\ell} \to 1$ for $T \to \infty$. If $\ell, \bar{\ell} = 0$ is inserted into (2.27), the thermal energy yields the Fermi-Dirac distribution of a particle with three times the energy and chemical potential of quarks. Hence, it can be identified with baryons in the confined phase. On the other hand, if (2.27) is evaluated for $\ell, \bar{\ell} = 1$, the thermal energy yields three times the Fermi-Dirac distribution of (single) quarks and the NJL expression is recovered. In this case, the potential describes the deconfined phase. Since, at $T = 0$, our model is equivalent to the model for which the parameters (2.21) were determined in [3], we can adopt those parameters. Analogously to (2.17) and (2.19), the values ℓ and $\bar{\ell}$ are determined by solving the stationary condition

$$\frac{\partial \Omega_{\mathrm{PNJL}}}{\partial \ell} = 0, \qquad \frac{\partial \Omega_{\mathrm{PNJL}}}{\partial \bar{\ell}} = 0. \qquad (2.28)$$

The model employed in the present work is identical to the one used in [7] except for the cutoff scheme. While, in [7], the three-momentum cutoff is only applied to the non-thermal part (the first term in the brackets) of the momentum integral in (2.27), the cutoff is applied to the whole integral in the present context.

2.3. Restrictions of the Model

Before proceed to the next section, we shall briefly recall some limitations of our model.

- The model parameters are fixed at $T = \mu = 0$ (cf. Sec. 2.1.3). In QCD, the interaction between quarks occurs by exchanging gluons, while the quark-quark interactions of the NJL model are only effective interactions. There is no reason to expect that the coupling constants of these effective interactions stay constant for all T and μ. As it is pointed out in [6], it should be expected, for instance, that the quark-quark coupling depends on the Polyakov loop.

- A great part of the strategy in constructing effective models is to pick the aspects which are relevant for a certain problem. As mentioned above, a CSC phase with diquarks as the relevant order parameters is predicted for low temperature and finite chemical potential (see [11] for a review). For three quark flavors, the diquark condensate can be defined as $\Delta_{AA'} \equiv \left\langle q^T \gamma_5 \lambda_A^f \lambda_{A'}^c q \right\rangle$, where $C \equiv i\gamma^2\gamma^0$ and λ_A^f and $\lambda_{A'}^c$ are the antisymmetric generators of flavor and color SU(3) symmetry, respectively, with $A, A' = 2, 5, 7$ [5]. Apparently, diquarks cannot be color neutral. Including both, the Polyakov loop and diquarks, into the same NJL-like model is a difficult - and so far an unsolved - task [32]. This point will be addressed again at the end of this work in Sec. 6.

- We have chosen to apply the mean-field approximation. This means that fluctuations are assumed to be small which is rather questionable especially near the phase transition. This point will be addressed in Sec. 4.1.2.

- The explicit representation of gluons has been reduced to the static Polyakov loop. Therefore, our model is not able (and does not aim) to reproduce the dynamics of gluons. The Polyakov loop should rather be interpreted as a tool that merely intends to describe the "shadow" of confinement cast on quarks.

Consequently, the success of the PNJL model in reproducing results from lattice calculations - even for higher-order fluctuations - is rather surprising. Nevertheless, the PNJL model provides us with a device to easily investigate the region around the critical point - a domain of the phase diagram that is not accessible for e.g. lattice QCD.

3. Phase Diagram

As already mentioned in the last section, the physical values of the condensates has to be determined for any temperature and chemical potential by solving the system of gap equations $\frac{\partial \Omega}{\partial \langle \rangle_i} = 0$ and choosing the solution with the lowest thermodynamic potential. The results for the PNJL model with $g_V = 0$ are illustrated in Figs. 3.1 and 3.2.

Considering Fig. 3.1(a), two different areas in the T-μ diagram can be identified: one with non-vanishing values of σ_u and one with $\sigma_u \approx 0$. Following [24], we refer to the first one as the Nambu-Goldstone (NG) phase and to the second one as the Wigner phase. One notes that although the difference between the phases is most pronounced for σ_u, differences are notable for all condensates. In the Nambu-Goldstone phase, we find that the chiral condensates take values of $\sigma_u = -1.504 \cdot 10^7 \, \mathrm{MeV}^3$ and $\sigma_s = -1.904 \cdot 10^7 \, \mathrm{MeV}^3$ which leads to constituent quark masses of $M_u = 335 \, \mathrm{MeV}$ and $M_s = 528 \, \mathrm{MeV}$ [3]. These masses are in good accordance with the constituent quark masses known for the hadronic phase of QCD. It can also be observed that the traced Polyakov loop vanishes which indicates confinement as discussed in the last section. The picture in the Wigner phase, however, is not as clear as in the Nambu-Goldstone phase. The only condensate taking a(n approximately) constant value is σ_u. In particular, it should be noted that ℓ and $\bar{\ell}$ are small for low T even in the Wigner phase. This observation is not only made for our model and other PNJL models [33], but is found to be even more distinct if one considers the limit of a large number of colors N_c [34].

In addition, two different kinds of transitions between the phases can be identified in Figs. 3.1 and 3.2. On the one hand, at low temperatures, the transition is characterized by a discontinuity in the order parameters. This type of phase transition is termed first-order phase transition. For low chemical potential, on the other hand, a cross-over - an analytical transition from one phase to the other occurs. Note that, since the cross-over is smooth, one should think of the transition as an area with a finite width instead of happening on a distinct line. The point where the first-order phase transition ends is commonly referred to as the critical (end) point (CP). Relating both scenarios to the thermodynamic potential Ω, the situation is found to be similar to the one sketched below (cf. [24]):
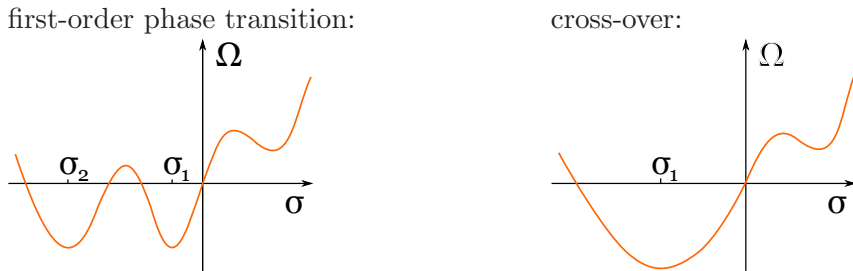
where we have simplified the problem to one order parameter σ. For the area near the first-order phase transition, a second minimum - besides the global one at σ_1 - is present at σ_2. As the phase transition is approached, $\Omega(\sigma_2) - \Omega(\sigma_1)$ becomes smaller, vanishes when the transition line is reached and becomes negative beyond the phase transition (meaning that, then, σ_2 is the global minimum). Near the CP, $\sigma_1 - \sigma_2$ decreases as the CP is approached and vanishes when the CP is reached (meaning that the minima are unified there). As for the cross-over (cf. right sketch), the transition is determined by only one minimum at σ_1. As one moves from one phase to the other, σ_1 continuously approaches the value of the target phase.

12
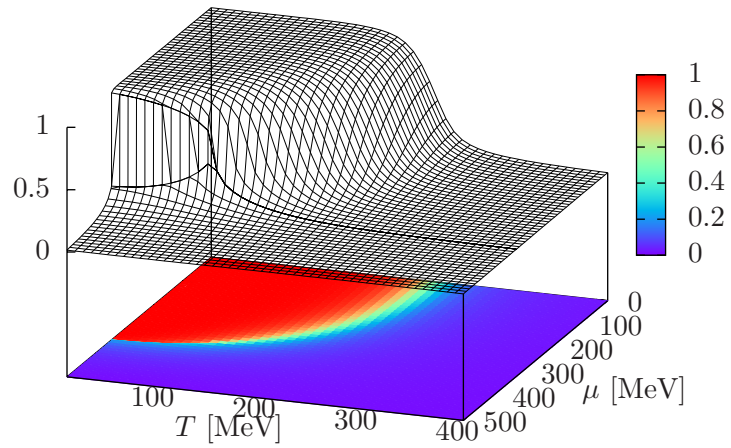
(a) $\sigma_u/(-1.504 \cdot 10^7 \text{ MeV}^3)$

(b) $\sigma_s/(-1.904 \cdot 10^7 \text{ MeV}^3)$

(c) ℓ
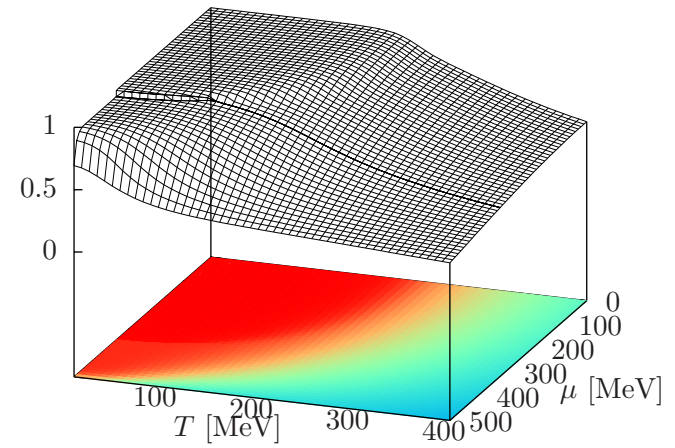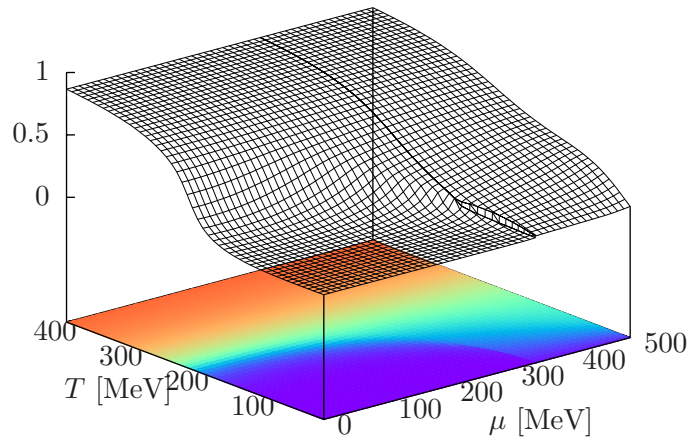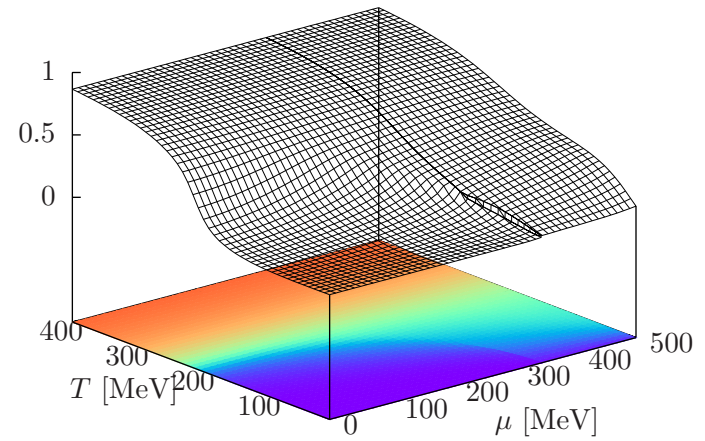
(d) $\bar{\ell}$

Figure 3.1: The solution of the gap equations for the various condensates in the PNJL model with $g_V = 0$ over the temperature T and the chemical potential μ. The chiral condensates are normalized to their values at $T = \mu = 0$. No normalization is applied for the Polyakov-loop order parameters.
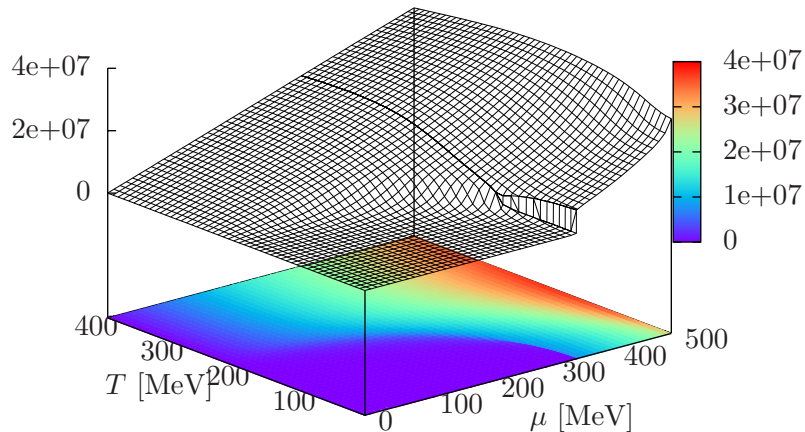
Figure 3.2: The quark number density ρ in units of $(\text{MeV})^3$ in the PNJL model with $g_V = 0$ over the temperature T and the chemical potential μ.

We have plotted the phase diagram for the PNJL model with $g_V = 0$ in Fig. 3.3(a). As for the cross-over, we have chosen to indicate it with the line where the chiral u-quark susceptibility χ_{uu}, which we will discuss in the next section, takes its maximum for a fixed ratio of T and μ. Note that there is no established criterion to draw a cross-over line and that choosing other criteria, for instance the line where σ_u takes 50% of its maximum value, yield slightly different results. It should be mentioned that, as it is done e.g. in [7], cross-over lines could also be drawn for the strangeness transition and the confinement-deconfinement transition. We have omitted them in Fig. 3.3(a), since, with their definition being rather arbitrary, such lines would carry only little information relevant for the further discussion.

As we have already seen in Fig. 2.1, the position of the critical point is highly sensitive to the chosen effective model and its parameters. Since the coupling constant of the vector interaction g_V will be varied, it is important to determine the critical point for each value. We have depicted the critical points for several values of g_V in Fig. 3.3(b). We remark that an increase in g_V makes the position of the critical point decrease in temperature and increase in chemical potential. A similar graph, where the coupling constant of the determinant interaction g_D has been varied, is shown in [7].

Note that a first-order phase transition and thus a critical point is only present in the model, if g_V is smaller than approx. $0.205g_S$. For this reason, we will vary g_V only up to $0.1g_S$ and not up to $0.25g_S$ as one would assume from Sec. 2.1.3.
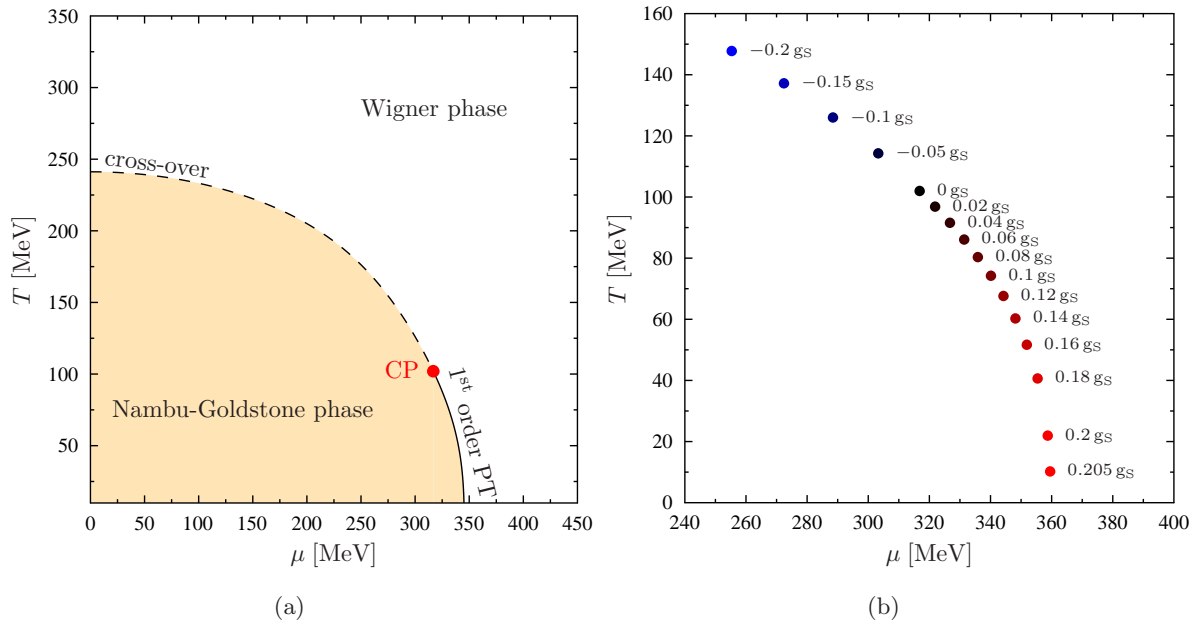
Figure 3.3: The phase diagram in the PNJL model without vector interaction (a) and the critical point(s) calculated in the PNJL model for different values of g_V (b). Numbers to the right of the points indicate the corresponding value of g_V.

4. Susceptibilities

In this section, we want to put the model developed in Sec. 2 to work and consider fluctuations. Although we have neglected fluctuation terms by applying the mean-field approximation, it is possible to calculate fluctuations as perturbations around the ground state. The susceptibilities χ_{ab} are quantities that are often used to treat lowest-order fluctuations and we define them as

$$\chi_{ab} \equiv \langle AB \rangle_c = -\frac{\mathrm{d}^2(\Omega/(VT))}{\mathrm{d}\mathfrak{m}_a \mathrm{d}\mathfrak{m}_b}, \tag{4.1}$$

where A, B are operators and a, b are the indices assigned to the respective susceptibilities (one for each derivation). $\mathfrak{m}_a$, $\mathfrak{m}_b$ are dimensionless mass terms connected to A and B by a term $\mathfrak{m}_a A$ in the Lagrangian. In our model, the term containing the explicit quark mass represents the aforementioned mass term for the chiral condensates, while the term containing the chemical potential takes this role for ρ. Note that we have to divide the explicit quark masses and the chemical potential by T to obtain the masses $\mathfrak{m}_a$, $\mathfrak{m}_b$ used in (4.1). So far, there are no mass terms for the Polyakov-loop order parameters immanent in our model. Therefore, we add a source term to the Polyakov-loop potential: $\Omega_{\mathrm{poly}} \to \Omega_{\mathrm{poly}} - TV(\eta\ell + \bar{\eta}\bar{\ell})$ with $\eta = \bar{\eta} = 0$ analogously to [7]. Summarizing the above, we can associate mass terms to each operator as shown in the table below. It should be noted that our definition differs from the "usual" definition used e.g. in

A	$\bar{u}u$, $\bar{d}d$	$\bar{s}s$	$\frac{1}{3}\mathrm{Tr}_c L$	$\frac{1}{3}\mathrm{Tr}_c L^\dagger$	$q^\dagger q$
$\langle A \rangle$	σ_u	σ_s	ℓ	$\bar{\ell}$	ρ
a	u	s	ℓ	ℓ	μ
$\mathfrak{m}_a$	$m_{u,d}/(2T)$	m_s/T	η	$\bar{\eta}$	μ/T

Table 4.1: Summary of the operators for which we calculate the susceptibilities, the notation we use for the corresponding thermal average and the index of the susceptibility as well as the mass term used for the differentiation in (4.1).

[3, 13, 16, 17, 19][1] by a factor T for the susceptibilities of the chiral condensate and the quark-number density. Since our definition is closer to the corresponding second-order fluctuations [13], it is probably the better choice for our application.

It can be shown that [16, 17]

$$\chi = -T \lim_{\vec{q} \to 0} \chi(0, \vec{q}) = -T \lim_{\vec{q} \to 0} \mathrm{Re}\Pi_{00}^R(0, \vec{q}) \tag{4.2}$$

with the response function $\chi(\omega, \vec{q})$ and the retarded Green's function of the response function

$$\Pi_{\mu\nu}^R(\omega, \vec{q}) = T \left[\mathrm{FT} \left(-i\theta(t) \left\langle [j_\mu(t, \vec{x}), j_\nu(0, 0)]_- \right\rangle \right) \right], \tag{4.3}$$

where FT denotes the Fourier transform, $\theta(t)$ the Heavyside function and $j_\mu(t, x)$ the current corresponding to the susceptibility. Due to the limit $\vec{q} \to 0$, susceptibilities are quantities representing fluctuations with a long (infinite) correlation length. Bearing in mind that the physics of fluctuations is a much wider field, we want to focus on this kind of fluctuations which are often termed the hydrodynamic modes.

---

[1]For instance, the quark-number susceptibility is defined as $\chi_{\mu\mu} = \frac{\partial\rho}{\partial\mu}$.

The actual calculation of the susceptibilities is straightforward. The total derivative of $\Omega/(VT)$ is calculated, the gap equations ((2.17), (2.19) and (2.28)) are applied and the resulting expression is differentiated once more to find

$$\chi_{ab} = -\frac{\partial^2(\Omega/(VT))}{\partial\mathfrak{m}_a\partial\mathfrak{m}_b} - \sum_i \frac{\partial^2(\Omega/(VT))}{\partial\mathfrak{m}_a\partial\langle\rangle_i}\frac{\mathrm{d}\langle\rangle_i}{\mathrm{d}\mathfrak{m}_b}, \tag{4.4}$$

where the sum runs over all condensates $\langle\rangle_i \in \{\sigma_u, \sigma_s, \ell, \bar{\ell}, \rho\}$. As the condensates themselves, their derivatives $\frac{\mathrm{d}\langle\rangle_i}{\mathrm{d}\mathfrak{m}_b}$ are determined by the gap equation. One now has to solve the system of linear equations which is obtained by differentiating the gap equations

$$\frac{\partial^2(\Omega/(VT))}{\partial\langle\rangle_j\partial\mathfrak{m}_b} + \sum_i \frac{\partial^2(\Omega/(VT))}{\partial\langle\rangle_j\partial\langle\rangle_i}\frac{\mathrm{d}\langle\rangle_i}{\mathrm{d}\mathfrak{m}_b} = 0. \tag{4.5}$$

4.0.1. Susceptibilities at $\mu = 0$

Before discussing the behavior of susceptibilities near the critical point, let us briefly discuss susceptibilities at $\mu = 0$. We have depicted some susceptibilities in Fig. 4.1. Since we want to
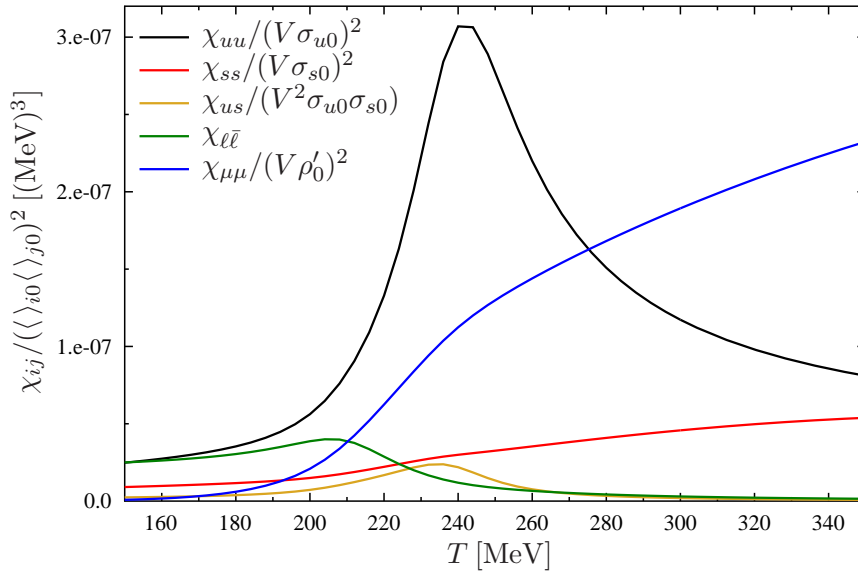
Figure 4.1: The susceptibilities of the two chiral condensates σ_u and σ_s, the quark number suscep-tibility $\chi_{\mu\mu}$ and the mixed susceptibilities for $\chi_{\ell\bar{\ell}}$ at $\mu = 0$. All susceptibilities, except $\chi_{\mu\mu}$, are normalized to the values given in (4.6). Since there is no maximum value for ρ, we arbitrarily set $\rho_0' = 10^7$ (MeV)^3. Additionally, all susceptibilities w.r.t. con-densates which have the unit of a density are normalized with corresponding factors of V.

compare the magnitudes of the various susceptibilities, we have scaled the values of the chiral and Polyakov-loop susceptibilities with corresponding factors of the maximum values of the

condensates

$$\sigma_{u0} = 1.504 \cdot 10^7 \ (\text{MeV})^3, \quad \sigma_{s0} = 1.904 \cdot 10^7 \ (\text{MeV})^3, \quad \ell_0 = \bar{\ell}_0 = 1. \tag{4.6}$$

As for the quark-number density ρ, there is no upper limit as it may be guessed from Fig. 3.2. Therefore, we arbitrarily choose to scale it with $\rho_0' = 10^7 \ \text{MeV}^3$. From Fig. 4.1, one immediately makes the following observations: Firstly, as it was already found in Fig. 3.1, the phase transition is most clearly represented in the chiral susceptibility of up-quarks χ_{uu}, while it is hardly noticeable for χ_{ss} and $\chi_{\mu\mu}$. Secondly, the peaks of the susceptibilities, for instance those of χ_{uu} and $\chi_{\ell\bar{\ell}}$, appear at different temperature. This can be interpreted as a hint that the chiral and the confinement-deconfinement phase transitions do not occur at the same temperature in our model. Note that the differences in the susceptibilities given here compared to those presented in [7] arise from the different cutoff scheme and from the different definition of susceptibilities. These two differences are also responsible for the fact that there is no peak apparent for χ_{ss} in Fig. 4.1, while it is clearly visible in [7].

4.1. Susceptibilities near the Critical Point

Let us now turn to the phase transition at finite μ. In Fig. 4.2, we have displayed the quark number susceptibility $\chi_{\mu\mu}$ on a mesh following the phase transition. It is observed that the susceptibility has a singularity at the CP. This feature is often used as a tool to determine the position of the critical point of a model and has also been used to determine the data for Fig. 3.3(b). Moreover, this singularity in susceptibilities has been suggested as a possible device to probe for the QCD critical point in heavy-ion collision experiments [15]. It is found that the peak is elongated along the phase transitions and that a discontinuity is apparent for the first-order phase transition. It is instructive to plot the susceptibility over the distance to the CP in a log-log plot as it is done in Fig. 4.3(b) for $\chi_{\mu\mu}$. It turns out that, close to the CP, the susceptibility is linear in the log-log plot and is thus proportional to r^a with the distance to the critical point r and the so-called critical exponent a. Depending on the direction from which the CP is approached, a takes different values. This dependence is well known [18, 35]. In mean-field theories, the critical exponent is known to be approximately 1 if the CP is approached parallel to the phase transition, while it is approximately $1 - 1/d$ with $d = 3$ being the dimension for any other direction. The fact that mean-field theories with the same symmetries share this feature is known as universality. Our results are displayed in Tab. 4.2. Note that the error given in

	first-order PT	Wigner phase	cross-over	NG phase
$g_V = 0$	-1.028(3)	-0.672(3)	-0.990(1)	-0.714(6)
$g_V = 0.05 g_S$	-1.028(3)	-0.668(4)	-0.989(1)	-0.718(6)
$g_V = 0.1 g_S$	-1.034(3)	-0.679(3)	-0.989(1)	-0.712(5)

Table 4.2: The critical exponents determined for the log-log plot of $\chi_{\mu\mu}$ (Fig. 4.3(b)) through a least-square fit. The values in brackets show the fitting error. If necessary, the functions were truncated at the right end such that the fitting errors are small.

brackets does only display the error returned from the fitting routine. For instance, the error in the determined value of the CP or non-critical contributions to the susceptibility may not be completely covered by the fitting error. The fact that we have defined the susceptibilities
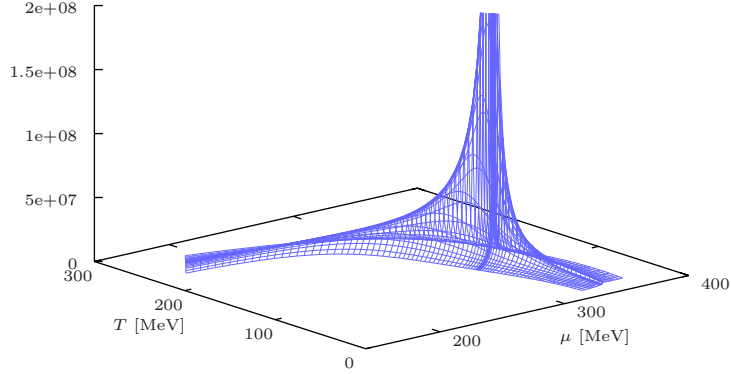
Figure 4.2: The quark number susceptibility $\chi_{\mu\mu}$ for the PNJL model with $g_V = 0$ in units of $V (\mathrm{MeV})^3$ plotted in an area around the phase transition with a width of $40\,\mathrm{MeV}$.

(a)

(b)
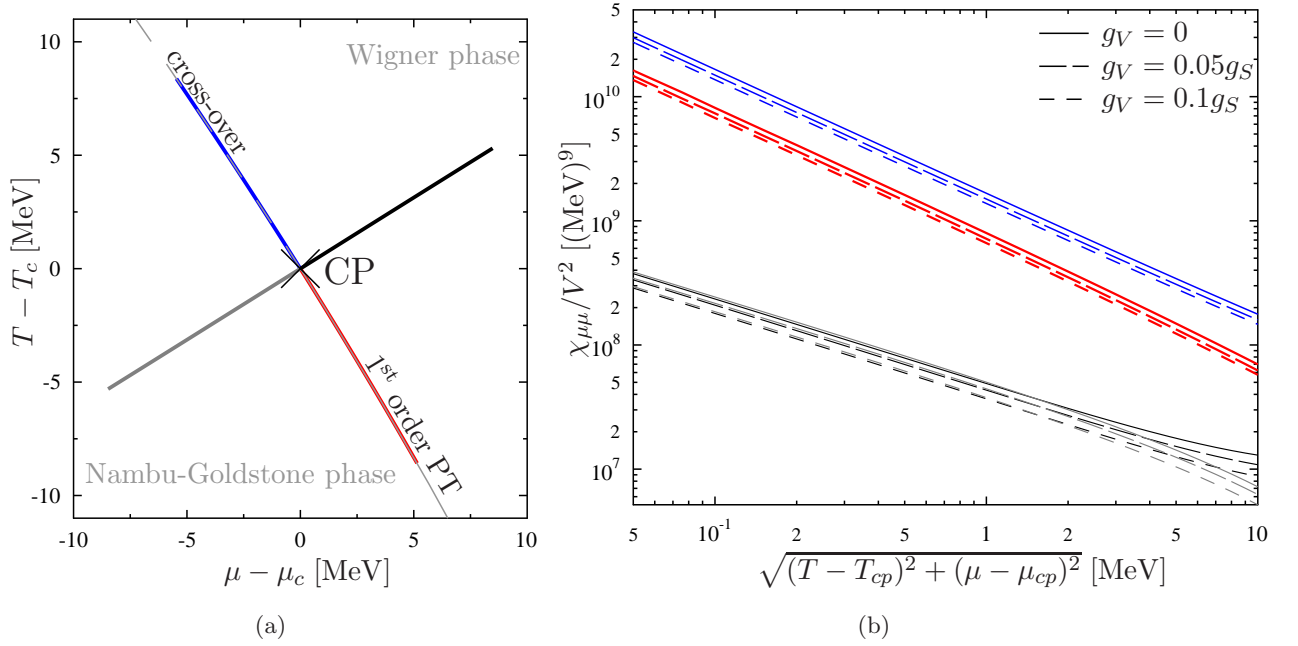
Figure 4.3: The quark number susceptibility $\chi_{\mu\mu}$ over the distance to the critical point as a log-log plot (b). The CP is apprached from the four directions displayed in (a): The red and the blue line depict an approach along the first-order phase transition (in the Wigner phase) and the cross-over, respectively. The black and the grey lines describe an approach perpendicular to the phase transition from the Wigner and the Nambu-Goldstone phase, respectively. The continuous lines mark the results for the PNJL without vector interaction, while the dashed lines mark results for the PNJL model with $g_V = 0.05 g_S$ and $g_V = 0.1 g_S$.

19
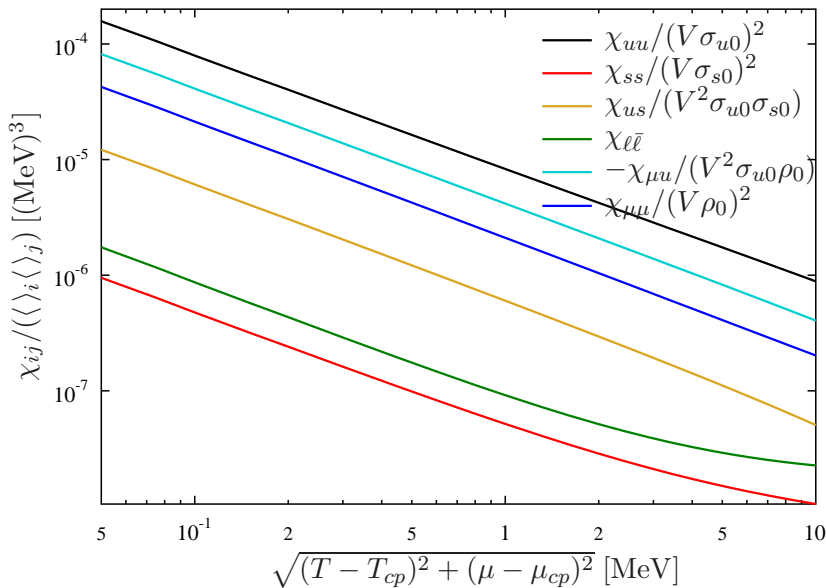
Figure 4.4: Various susceptibilities along the first-order phase transition. The susceptibilities are normalized according to (4.6) and (4.7). Again, we have additionally normalized the condensates which have units of a density with factors of V

differently from the usual definition mentioned at the beginning of this section is found to lead to a deviation of about 2%.

We do not find any evidence that the vector interaction has an influence on the critical exponent[2], while it clearly does have an influence on the total magnitude of the susceptibilities. We find the magnitude to be diminished for increasing g_V. Note that, with the usual definition of susceptibilities mentioned above, susceptibilities become enhanced and that the discrepancy is due to the fact that the critical point decreases in temperature for increasing g_V. This enhancement becomes even stronger, if one considers dimensionless susceptibilities used in [7], where factors of T are multiplied such that the susceptibilities become dimensionless.

Note that the divergence described above is not unique to the quark number susceptibility, but is observed - more or less pronounced - for all susceptibilities. We have illustrated this for some selected susceptibilities calculated for an approach along the first-order phase transition in Fig. 4.4, where we have used (4.6) and

$$\rho_0 = \frac{N_f N_c}{3}\left(\frac{\mu^3}{\pi^2} + T^2\mu\right) \tag{4.7}$$

to normalize the susceptibilities.

---

[2]This does not come as a surprise, since the value of the vector-interaction coupling constant does not influence the character of the model.
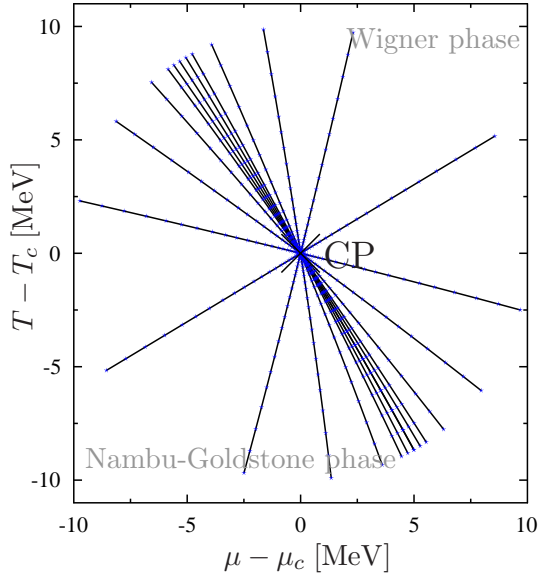
Figure 4.5: The mesh on which we determine the critical mode.

4.1.1. Critical Mode

Let us now consider the mechanism which leads to the behavior described above. It is possible to rewrite (4.4) and (4.5) into one expression

$$\chi_{ab} = -\frac{\partial^2(\Omega/(VT))}{\partial \mathfrak{m}_a \partial \mathfrak{m}_b} - \sum_{i,j} \frac{\partial^2(\Omega/(VT))}{\partial \mathfrak{m}_a \partial \langle\rangle_i} \left(\frac{\partial^2(\Omega/(VT))}{\partial \langle\rangle \partial \langle\rangle}\right)^{-1}_{i,j} \frac{\partial^2(\Omega/(VT))}{\partial \langle\rangle_j \partial \mathfrak{m}_b}, \qquad (4.8)$$

where $\frac{\partial^2(\Omega/(VT))}{\partial \langle\rangle \partial \langle\rangle}$ is the Hessian matrix of $\Omega/(VT)$. Apparently, if the susceptibilities have a singularity it must arise from the Hessian matrix as long as Ω is analytic. The fact that the singularity arises at the critical point can be easily elucidated if one considers the Landau theory [13], where we only have one order parameter. In this situation which basically corresponds to that sketched in Sec. 3, the two minima responsible for the first-order phase transition evidently merge at the critical point, since the solution of the gap equations is continuous beyond the CP. Then, the distance between the two equivalent minima is infinitesimal and the curvature has to be 0. Since the curvature corresponds to the Hessian matrix in (4.8), this does inevitably lead to a singularity in the susceptibilities.

However, our model accommodates several order parameters. Hence, it is interesting to investigate what kind of excitation from equilibrium is responsible for the singularity. In order to accomplish this, we have to identify the eigenvalue that becomes 0 at the critical point and the corresponding eigenvector. This eigenvector is commonly referred to as the critical or soft(ening) mode.

For this investigation, we supplement the mesh from Fig. 4.3(a) with additional data points and evaluate the eigensystem for a mesh as it is given in Fig. 4.5. Again, we normalize the Hessian matrix by factors of (4.6) and (4.7) and carry out the calculation for $g_V = 0.01g_S$ and $g_V = 0.1g_S$ to identify the eigenvalues which become 0 at the CP and are depicted in Fig. 4.6 with those of the critical modes. We find that the eigenvalues differ only slightly in magnitude which

(a) $g_V = 0.01g_S$ (b) $g_V = 0.1g_S$
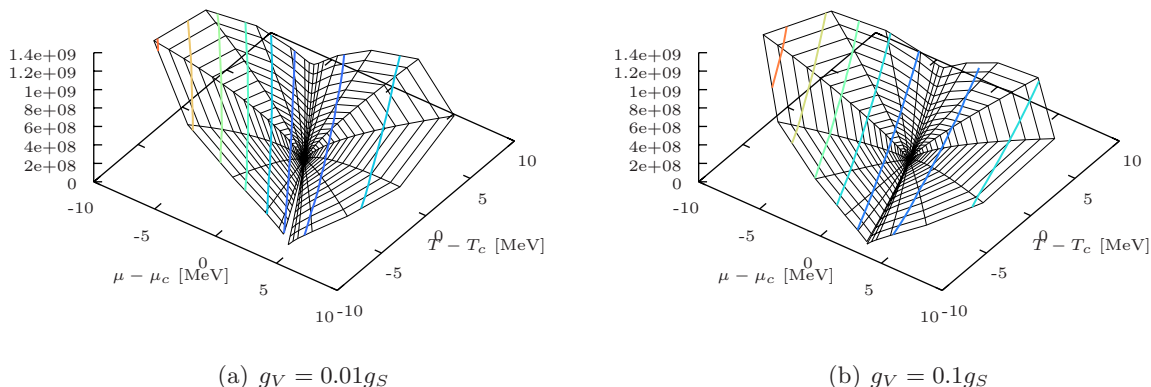
Figure 4.6: The eigenvalue of the matrix $\frac{\partial^2 \Omega}{\partial \langle\rangle_i \partial \langle\rangle_j}$ which is responsible for the softening behaviour, i.e. the eigenvalue goes to zero near the critical point. Colored lines mark the heights labeled on the z-axes.

is not surprising at all, since the scaling behavior found in Fig. 4.4 has no strong dependence on g_V. Considering the corresponding eigenvector, we find that its components strongly depend on the vector interaction. We have illustrated the components of the normalized eigenvector for $g_V = 0.01g_S$ and $g_V = 0.1g_S$ in Figs. 4.7 and 4.8. For both values of g_V, we find that σ_u has the largest contribution to the eigenvector while the contribution from σ_s is rather small. The contributions from ℓ and $\bar{\ell}$ seem to be of some importance in the NG phase, while they vanish as the phase transition is approached and their influence seems to be negligible in the Wigner phase. Hence, the critical mode seems to be determined primarily by fluctuations in $\bar{u}u$, $\bar{d}d$ and $q^\dagger q$. The fluctuations in the quark number susceptibility gain importance near the CP. One observes that this gain is rather steep for $g_V = 0.01g_S$ and widespread for $g_V = 0.1g_S$. We conclude that the signature of the CP in the critical mode takes a larger area of the phase diagram if g_V is large.

4.1.2. Ginzburg-Levanyuk Criterion

In this section, we want to inspect whether the mean-field approximation introduced in Sec. 2.1.1 is a legitimate approximation or not. For this purpose, we succinctly review the Ginzburg-Levanyuk criterion following [13] and will discuss it afterwards. For simplicity, we again consider a Landau theory with only one order parameter σ. Then, we can expand the thermodynamic potential in σ for given (μ, T) around the equilibrium state as

$$\Omega(\Delta\sigma)/V = \Omega_0 + (\Delta\sigma)^2 a + (\Delta\sigma)^4 b. \tag{4.9}$$

Since fluctuations occur locally, we also have to expand Ω with respect to spatial derivatives of σ. Nevertheless, because we are only interested fluctuations with a long wavelength, it is sufficient to add a term

$$\mathfrak{g}\left(\nabla(\Delta\sigma)\right)^2, \tag{4.10}$$
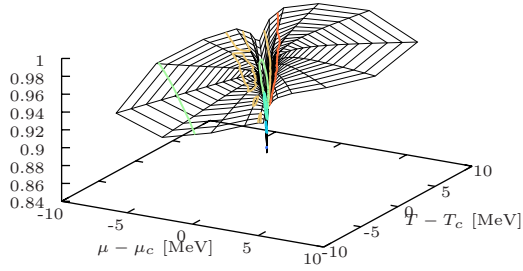
(a) σ_u-component, $g_V = 0.01g_S$.
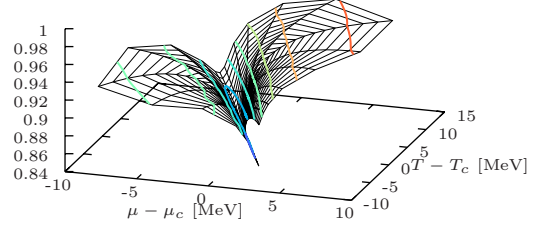
(b) σ_u-component, $g_V = 0.1g_S$.
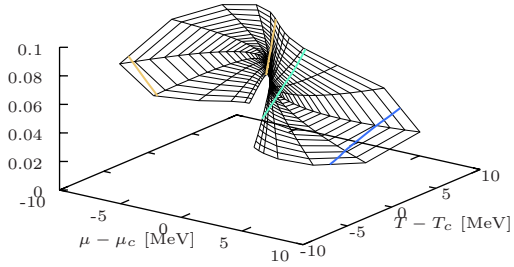
(c) σ_s-component, $g_V = 0.01g_S$.
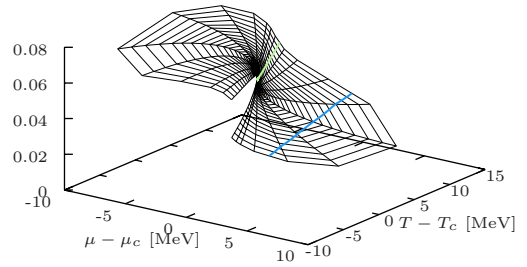
(d) σ_s-component, $g_V = 0.1g_S$.
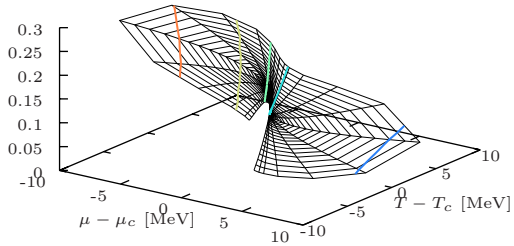
(e) ℓ-component, $g_V = 0.01g_S$.
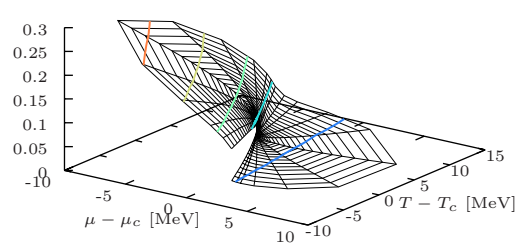
(f) ℓ-component, $g_V = 0.1g_S$.

Figure 4.7: The σ_u-, σ_s- and ℓ-components of the eigenvector corresponding to the critical mode for $g_V = 0.01g_S$ and $g_V = 0.1g_S$ presented in Fig. 4.6. Colored lines mark the heights labeled on the z-axes. The eigenvector is normalized to a length of 1.
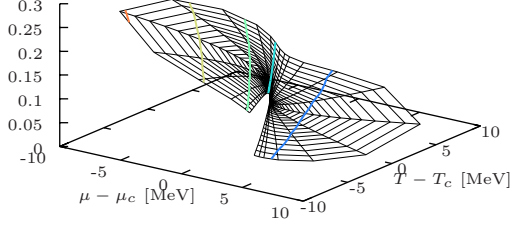
(a) $\bar{\ell}$-component, $g_V = 0.01 g_S$.
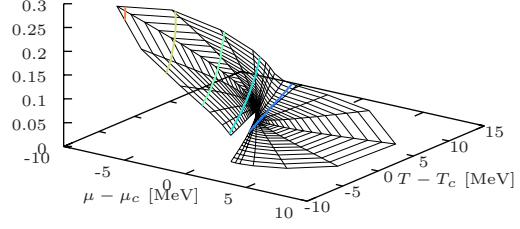
(b) $\bar{\ell}$-component, $g_V = 0.1 g_S$.
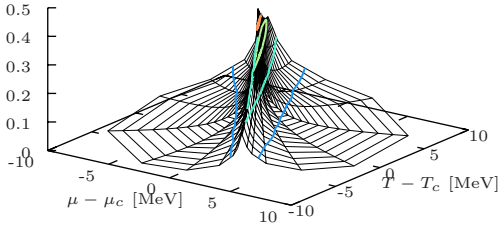
(c) ρ-component, $g_V = 0.01 g_S$.
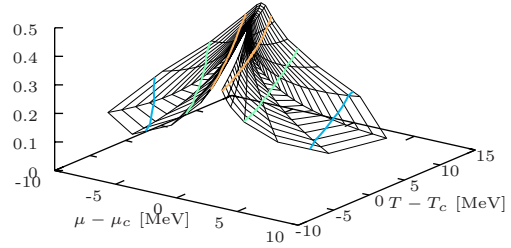
(d) ρ-component, $g_V = 0.1 g_S$.

Figure 4.8: The $\bar{\ell}$- and ρ-components of the eigenvector corresponding to the critical mode for $g_V = 0.01 g_S$ and $g_V = 0.1 g_S$ presented in Fig. 4.6. Colored lines mark the heights labeled on the z-axes. The eigenvector is normalized to a length of 1.

where cubic symmetry is assumed[3]. Requiring that a homogenous body is stable, $\mathfrak{g} > 0$ has to hold. Conversely speaking, if $\mathfrak{g} < 0$, the physically preferred phase is inhomogeneous. The part of the potential which is responsible for fluctuations can thus be written as

$$\Delta\Omega = \int \mathrm{d}V \left[a(\Delta\sigma)^2 + \mathfrak{g}\left(\nabla(\Delta\sigma)\right)^2 \right] = V \int \frac{\mathrm{d}^3 k}{(2\pi)^3} (\mathfrak{g}k^2 + a)\widetilde{\Delta\sigma}(\vec{k})\widetilde{\Delta\sigma}(-\vec{k}). \tag{4.11}$$

For the second step, a Fourier transformation has been applied. Calculating the expectation value of $\Delta\sigma_{\vec{k}}\Delta\sigma_{-\vec{k}}$ from the partition function yields the intermediary result

$$\left\langle \widetilde{\Delta\sigma}(\vec{k})\widetilde{\Delta\sigma}(-\vec{k}) \right\rangle = \frac{T}{2V(\mathfrak{g}k^2 + a)}. \tag{4.12}$$

With the help of this relation, the correlation function

$$G(\vec{r}) = \left\langle \Delta\sigma(\vec{0})\Delta\sigma(\vec{r}) \right\rangle = V \int \frac{\mathrm{d}^3 k}{(2\pi)^3} \left\langle \widetilde{\Delta\sigma}(\vec{k})\widetilde{\Delta\sigma}(-\vec{k}) \right\rangle e^{i\vec{k}\vec{r}} = \frac{T}{8\pi\mathfrak{g}r} e^{-r/r_c}, \tag{4.13}$$

---

[3] All first-order and all other second-order terms can be included into $\mathfrak{g}$ or contribute only as surface terms after volume integration.

where $r_c = \sqrt{\frac{\mathfrak{g}}{a}}$ is the correlation radius, can be evaluated.

Now, the Ginzburg-Levanyuk criterion can be formulated. To ensure that fluctuations are sufficiently small so that the MFA is a good approximation, the mean square fluctuation (the susceptibilities defined in (4.1)) averaged over the correlation volume r_c^3 is required to be small compared to the magnitude of σ^2 which is estimated as a/b. Applying that the mean square fluctuation is of order $\frac{T}{aV}$ in the expansion (4.9), we readily arrive at the Ginzburg-Levanyuk criterion

$$\frac{T^2 b^2}{\mathfrak{g}^3 a} \ll 1. \tag{4.14}$$

Before employing the criterion, we have to translate (4.14) to our model. From the discussion in Sec. 4.1.1, it is apparent that the eigenvector of the critical mode takes over the role of the order parameter σ in the Landau theory. Consequently, a and b are obtained by calculating the second and the fourth derivative of the thermodynamic potential in direction of the eigenvector, respectively. However, obtaining $\mathfrak{g}$ is much more involved and it already has been done for the NJL model in [17]. Because the calculation is rather lengthy and tedious, we only outline the general procedure here and present the differences compared to [17] and the resulting formulas in Appendix A. As for contributions of the chiral-condensates and the quark-number density, the thermodynamic potential is expanded in $\overline{q}q$ and $q^\dagger q$ and the second-order terms - the polarization functions - are considered. It should be noted that this has to be done before the trace operation. Differentiating the momentum-space polarization function with respect to the momentum twice and putting $q = 0$ afterwards yields the contributions of the chiral condensates and the quark number density. Nevertheless, determining the contributions of the gauge field is not an easy task. In Sec. 2.2, we have introduced the Polyakov loop as a rather abstract non-local order parameter. As a consequence, an approach similar to that of the quark contributions is not applicable here. For this reason, we confine ourselves to the quark contributions to $\mathfrak{g}$. Recalling that the contributions of the Polyakov loop to the eigenvector of the critical mode are comparably small, we may assume that the error made by neglecting the Polyakov loop contributions is not too big.

As we have already done in the last subsection, we evaluate the expansion coefficients necessary to calculate the Ginzburg-Levanyuk criterion on the mesh given in Fig. 4.5. Then, the second-order coefficient a is given by the eigenvalue of the critical mode (Fig. 4.6). The results for the fourth-order coefficient b and the coefficient of the derivative $\mathfrak{g}$ are illustrated in Fig. 4.9.

For $\mathfrak{g}$, we find that it approaches 0 near the critical point and is small along the phase transition. As we have observed for the critical mode, here, too, a stronger coupling of the vector interaction leads to a smoother decrease. For $g_V = 0.1 g_S$, $\mathfrak{g}$ is observed to even change its sign in a small area of the phase diagram (indicated by the orange line in Fig. 4.9(b)), a behavior which is at first unexpected. This could be explained by the fact that the sign change only happens in the NG phase, and this behavior might thus be caused by the missing contributions from ℓ, $\overline{\ell}$. Although these contributions could make $\mathfrak{g}$ (taken in the direction of the critical mode) positive, the implication that the favored phase is inhomogeneous for some components suggests that it is inhomogeneous for all components - even if our model predict $\mathfrak{g} > 0$ for other components. This is because our model is incapable of dealing with inhomogeneous phase. Nevertheless, there are calculations in the NJL model considering inhomogeneous phases which also exhibit a change of sign near the critical point. This means that the preferred phase might in fact be inhomogeneous. According to [36], in some areas of the phase diagram, the phase transition (as displayed in Fig. 3.3(a)) should be substituted with two second-order phase transition lines
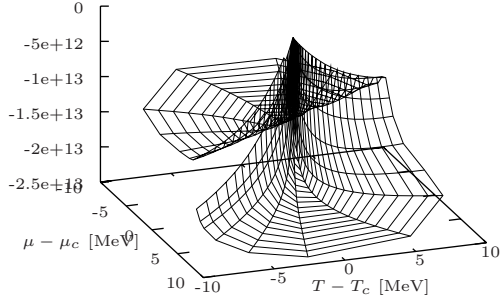
(a) $-g$, $g_V = 0.01g_S$
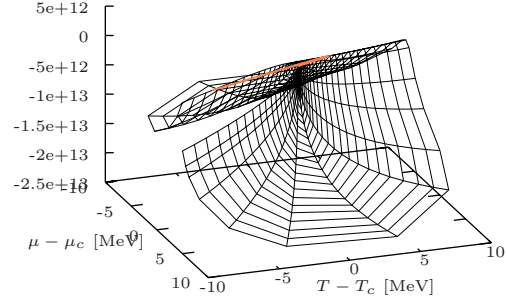
(b) $-g$, $g_V = 0.1g_S$
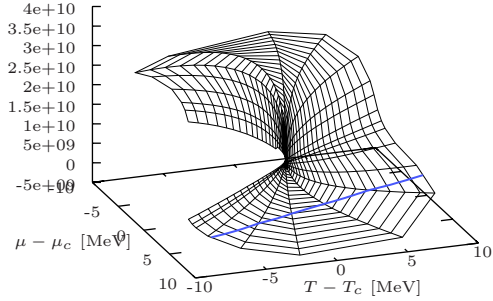
(c) b, $g_V = 0.01g_S$
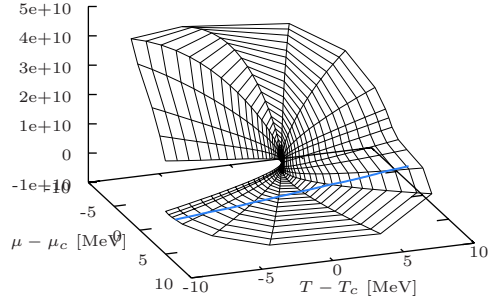
(d) b, $g_V = 0.1g_S$

Figure 4.9: The quark contributions to expansion coefficient $\mathfrak{g}$ ((a) and (b)) and the expansion coefficient b ((c) and (d)). Colored lines mark sign changes of the functions.

delimiting the inhomogeneous phase. The point where these two lines then intersect is referred to as Lifshitz point. Calculations in the NJL model have shown that for $g_V = 0$, the critical point coincides with the Lifshitz point. The CP is found inside the inhomogeneous phase[4] for $g_V > 0$ since the Lifshitz point does not decrease in temperature for increasing g_V [37]. Our finding of a sign change only for $g_V = 0.1g_S$ and not for the rather small $g_V = 0.01g_S$ might reflect the results of [37]. However, it should be noted that, in the present study, $\mathfrak{g}$ is only evaluated in direction of the critical mode and that, thereofore, Figs. 4.9(a) and (b) do not allow an in depth discussion of inhomogeneous phases.

As a side note, it is interesting to note that the fourth-order coefficient b changes its sign close to the critical point - as it is displayed by the blue line in Figs. 4.9(c) and (d). This may be understood as a indication that our model is close to a massless theory (i.e. $m_{u,d} = m_s = 0$),

---

[4]It should be clarified that, in this case, the critical point does not exist, if the inhomogeneous phase is considered. The critical point to which we refer here is the critical point which is found, if the inhomogeneous phase is not considered.

where the critical point turns into a tricritical point (TCP). In that case, b would have to be 0 at the (tri)critical point.

Calculating the Ginzburg-Levanyuk criterion for the expansion coefficients given above, we obtain Fig. 4.10. Defining the critical region as the region in the phase diagram where the
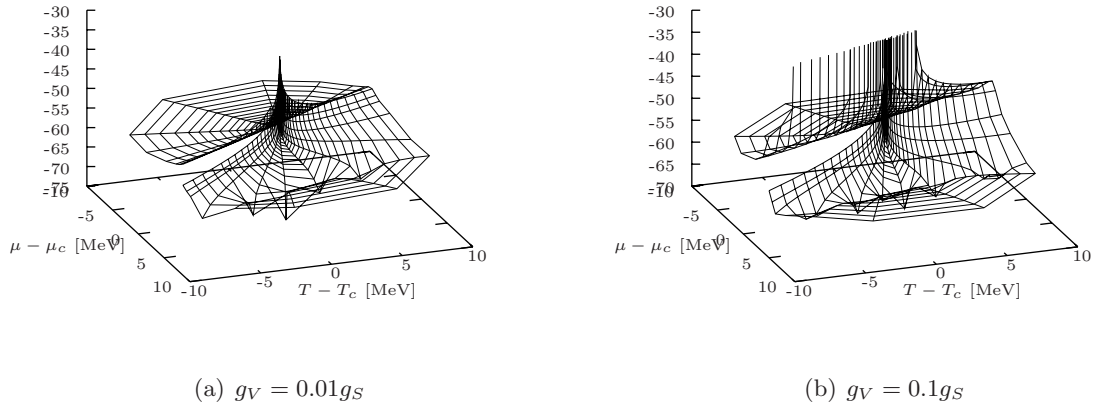
(a) $g_V = 0.01g_S$

(b) $g_V = 0.1g_S$

Figure 4.10: The left hand side of the Ginzburg-Levanyuk criterion (4.14) for $g_V = 0.01g_S$ and $g_V = 0.1g_S$ plotted with a logarithmic z-axis. The divergence for $g_V = 0.1g_S$ is due to the change of sign in $\mathfrak{g}$.

Ginzburg-Levanyuk criterion is not small, we observe that the critical region occupies a rather small area of the phase diagram. Near the cross-over, we again find enhanced values for $g_V = 0.1g_S$ compared to $g_V = 0.01g_S$. As a consequence of change of sign in $\mathfrak{g}$, their exists a small region around the CP which is stretched along the phase transition in the NG phase, where the Ginzburg-Levanyuk criterion diverges. As mentioned above, $\mathfrak{g} < 0$ implies that inhomogenous phases are preferred which contradicts our model, since we have assumed global order parameters. Hence, it is only consistent that the Ginzburg-Levanyuk criterion deems our model to be a bad approximation in this region of the phase diagram. Departing from the CP into the Wigner phase, the behavior of the Ginzburg-Levanyuk criterion is mainly determined by the fourth-order coefficient b changing its sign and the behaviors for $g_V = 0.01g_S$ and $g_V = 0.1g_S$ resemble each other.

Since the ratio b/a was introduced as a characteristic magnitude of the order parameter, the case that b/a vanishes should be ruled out in a model where the CP is almost a TCP. For instance, if the sixth-order expansion coefficient c is available, one could substitute b/a with $\sqrt{(b/a)^2 + c/a}$ to circumvent the problem. However, the unknown contribution of the Polyakov loop to $\mathfrak{g}$ poses a much bigger problem in evaluating the Ginzburg-Levanyuk criterion, since only small contributions to $\mathfrak{g}$ are necessary to significantly change the result presented int Fig. 4.10 - particularly the size of the region where the criterion diverges. Nevertheless, it seems to be save to conclude that a stronger vector interaction leads to a broader critical region. We also observe that the critical region - and thus the region where the MFA is a bad approximation - is a (rather small) region around the CP which is stretched along the phase transition. This fact does not come as a surprise since, in the MFA, susceptibilities can only be treated as perturbations from the ground state.

5. Higher Moments

In this section, we want to investigate higher-order fluctuations - i.e. the third and fourth moments[5]. Recently, both have been suggested as possible probes for the QCD critical point in heavy-ion collision experiments. For instance, it has been suggested that, contrary to susceptibilities, third moments change their sign as rhe phase transition is crossed which may allow for additional information being gained from experimental data [20]. In addition, higher-order fluctuations diverge with a higher critical exponent than susceptibilities and might thus give stronger hints on the position of the CP in the phase diagram than susceptibilities [21]. As another important application, higher-order moments are often used to check whether effective theories are able to reproduce lattice calculations [9, 38]. Since lattice calculations are limited to $\mu = 0$, higher-order moments w.r.t. μ are crucial because they allow for expansions to finite chemical potential. In this case, the focus is put on the behavior of moments (also of even higher order) on the T-axis. In the present study, we are interested in the first application and investigate how third and fourth moments behave near the critical point.

We define the third and the fourth moments in analogy to the susceptibilities as

$$\chi_{abc} \equiv \langle ABC \rangle_c = -\frac{\mathrm{d}^3(\Omega/(VT))}{\mathrm{d}\mathfrak{m}_a \mathrm{d}\mathfrak{m}_b \mathrm{d}\mathfrak{m}_c} \qquad \text{and} \tag{5.1}$$

$$\chi_{abcd} \equiv \langle ABCD \rangle_c = -\frac{\mathrm{d}^4(\Omega/(VT))}{\mathrm{d}\mathfrak{m}_a \mathrm{d}\mathfrak{m}_b \mathrm{d}\mathfrak{m}_c \mathrm{d}\mathfrak{m}_d} \tag{5.2}$$

with the masses $\mathfrak{m}_a \ldots \mathfrak{m}_d$ outlined in Tab. 4.1. They are calculated by further differentiating (4.4). Similarly to $\frac{\mathrm{d}\langle\rangle_i}{\mathrm{d}\mathfrak{m}_b}$ in Sec. 4, the derivatives $\frac{\mathrm{d}^2\langle\rangle_i}{\mathrm{d}\mathfrak{m}_b \mathrm{d}\mathfrak{m}_c}$ and $\frac{\mathrm{d}^3\langle\rangle_i}{\mathrm{d}\mathfrak{m}_b \mathrm{d}\mathfrak{m}_c \mathrm{d}\mathfrak{m}_d}$ are obtained by inverting derivatives of the gap equations. Since this is straightforward but rather lengthy, we omit the corresponding formulas here, but give them in Appendix B. It should be noted that, in general, the method described in the Appendix can easily be extended to arbitrarily high orders. However, with increasing order more and more derivatives of Ω are needed for the evaluation. In order to allow for an easier coding of the numerical calculations of the higher-order moments, we have employed the method of "automatic differentiation" (AD) [39].

5.1. Third and Fourth Moments near the Critical Point

To investigate the behavior in the vicinity of the critical point, it is instructive to not only evaluate the higher-order moments in radial direction but also on a circle around the critical point. In Fig. 5.1, we present the susceptibilities, the third and fourth moments of the quark number susceptibilities for $g_V = 0, 0.05g_S, 0.1g_S$ on a circle around the respective critical points with a radius of $0.1\,\mathrm{MeV}$.

As it could be expected from the discussion in the last section, the susceptibilities have a peak at both phase transitions. As pointed out in [20], we observe that the third moments are negative on the side of the phase transition that lies in the Wigner phase and are positive on the side of the NG phase. As for the fourth moments, we find two small positive peaks separated by a narrow but much larger negative peak at the cross-over, while we observe a single peak at the first-order phase transition. As for the different coupling strengths of the vector interaction, we

---

[5]In literature, the third moments are sometimes referred to as the "skewness" and the fourth moment as the "kurtosis". In this work, we, however, will only use the terms third and fourth moments.
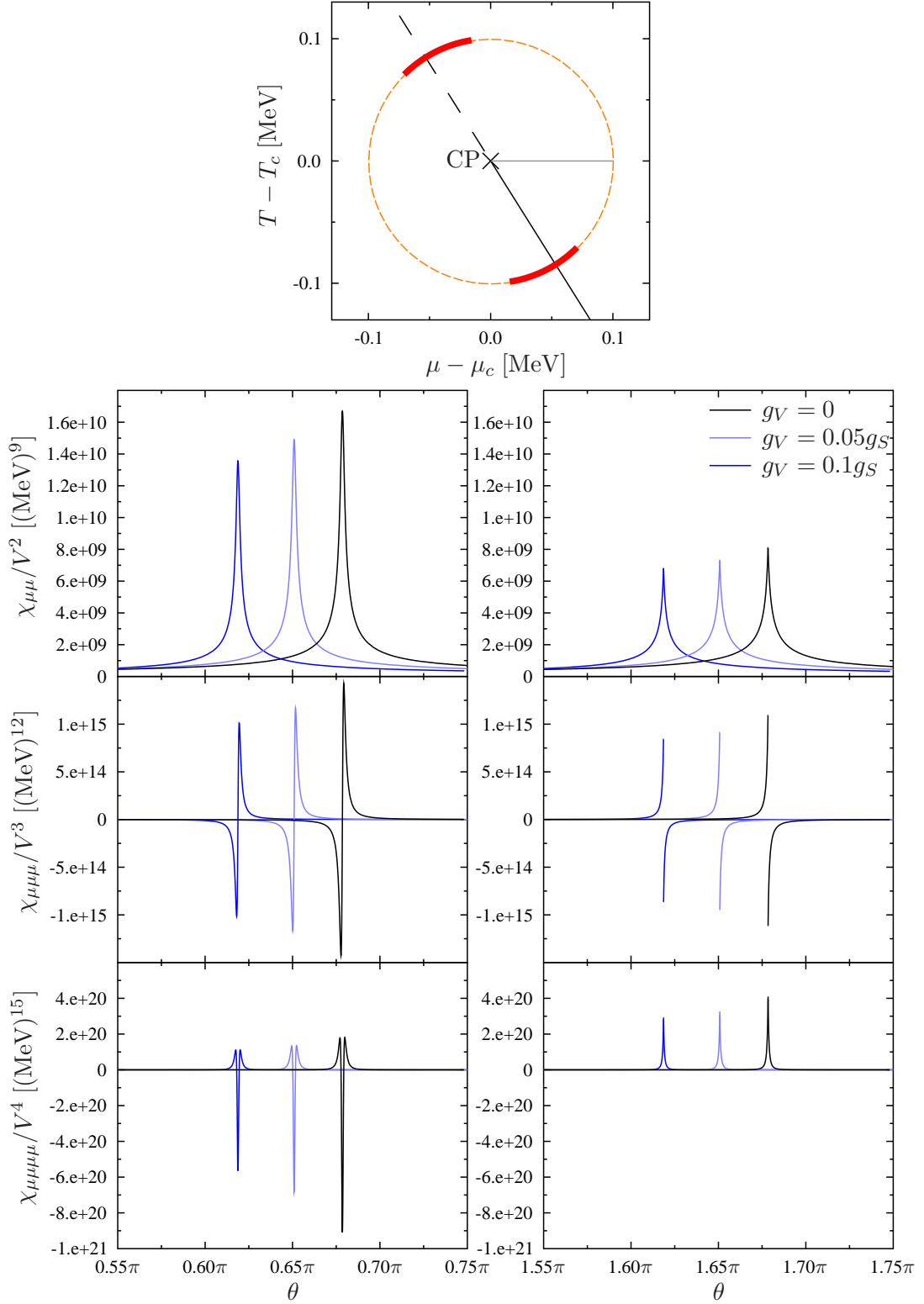
Figure 5.1: The lower graphs show the susceptibility, the third and the fourth moment of the baryon-number density evaluated on the thick red lines marked in the upper panel. θ is the angle enclosed with the grey line in the upper panel. Hence, the left side shows the cross-over, while the first-order phase transition is displayed on the right side.
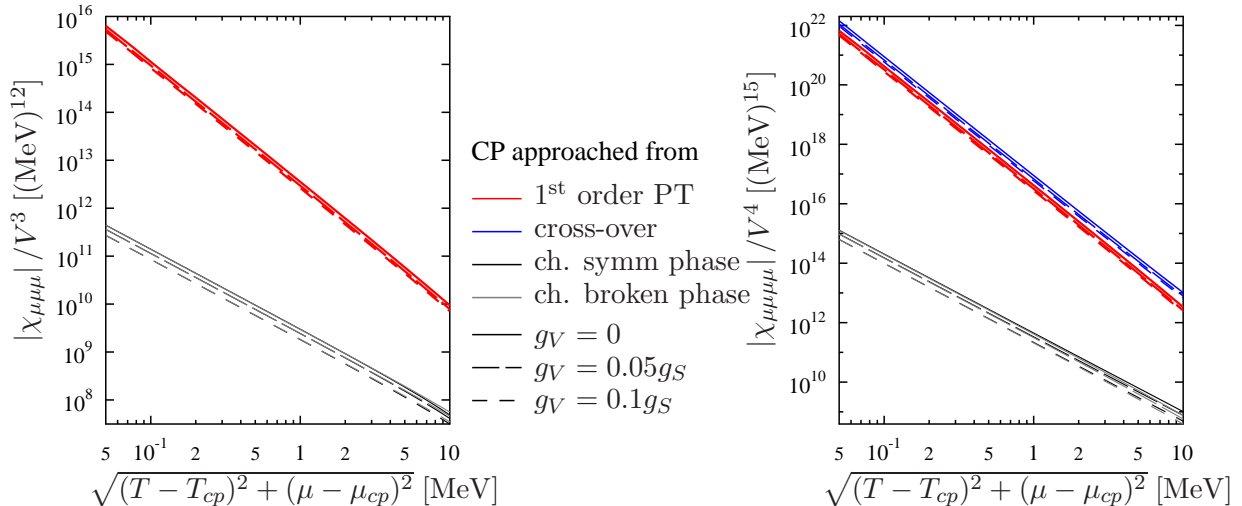
Figure 5.2: The third and the fourth moments of the baryon-number density over the distance to the critical point as a log-log plot.

find that all moments are diminished for increasing g_V. The different positions of the peaks is due to the different angles in which the phase transitions traverse the critical point.

The result found for the cross-over can be understood easily, if one regards the susceptibilities and the third and fourth moments as functions of μ instead of functions of the angle θ. This is plausible since, along the red lines in the upper panel of Fig. 5.1, a change of the angle is mostly made up of a change in μ. Thinking of the peak in the susceptibility as a Gaussian, the behavior of the third and the fourth moments resemble those of the first and second derivative of a Gaussian.

Considering the first-order phase transition, we again interpret the susceptibility as a function of μ and the third and fourth moments as its derivatives. Owed to the discontinuity at the phase transition, the third moments change their sign discontinuously. As a consequence not negative peak in the fourth moments.

Let us now consider the behavior of the third and fourth moments if the critical point is approached in radial direction. Evaluating the functions on the lines given in Fig. 4.3(a) and plotting them again in a log-log plot over the distance to the critical point, we find Fig. 5.2. For the third moment, we have omitted the line for the cross-over, because the line on which the moments are evaluated runs between the positive and negative peak displayed in the left panel for $\chi_{\mu\mu\mu}$ in Fig. 5.1.

We again find that the divergence is proportional to r^α with r being the distance to the critical point and α the critical exponent which we have displayed in Tab. 5.1. As we have already found for the susceptibilities, it turns out that g_V influences the magnitude of the moments but not their critical exponents. We observe that the critical exponents are approximately increased by 1 for the directions perpendicular to the phase transition, while they are increased by approximately 1.5 if the CP is approached along the phase transition. We also want to compare our result with the relation between critical exponents predicted in [21] (which is also implied by scaling and universality)

$$\left\langle (\delta N_B)^k \right\rangle_c \propto \xi^{k(5-\eta)/2-3}, \tag{5.3}$$

30

$\chi_{\mu\mu\mu}$	first-order PT	Wigner phase	NG phase	
$g_V = 0$	-2.531(2)	-1.698(6)	-1.684(3)	
$g_V = 0.05 g_S$	-2.530(2)	-1.695(4)	-1.683(2)	
$g_V = 0.1 g_S$	-2.529(0)	-1.694(4)	-1.681(2)	

$\chi_{\mu\mu\mu\mu}$	first-order PT	Wigner phase	cross-over	NG phase
$g_V = 0$	-4.040(5)	-2.665(1)	-3.978(3)	-2.697(3)
$g_V = 0.05 g_S$	-4.038(5)	-2.651(1)	-3.978(3)	-2.695(3)
$g_V = 0.1 g_S$	-4.037(4)	-2.654(1)	-3.979(3)	-2.690(3)

Table 5.1: The critical exponents α for the third (upper table) and fourth (lower table) moments of the quark number density for the critical point being approached from the directions displayed in Fig. 4.3(a). Note that the errors given in brackets only represent the errors of the least-square fit.

where N_B is the baryon number, k the order of the moment, ξ the correlation length and a constant $\eta \ll 1$. Relating our higher-order critical exponents with those determined for the susceptibility, we can determine η. With this procedure, we find $\eta \approx 0.2 \ldots 0.5$. However, theses values are very sensitive to errors in the critical exponents. For instance, changing the critical exponent of the susceptibility for the approach along the first-order phase transition from 1.03 to 1.05, decreases η from 0.45 to 0.33. As mentioned above, the errors in the critical exponents are probably larger than those given in the tables. Although our values of η are rather high, our results still reflect the general behavior of [21].

Although we have presented only the results for the quark-number density, the same features are also found for all other higher moments like χ_{uuu}, χ_{uuuu} and we, therefore, omit them here. Note that this also holds for the moments evaluated on a circle around the CP, where we have observed that the third and fourth moments act like derivatives w.r.t. μ.

5.2. The Fourth Moment as a Probe in Experiments

Although discussing all processes that lead to the results of experimental measurements is beyond the scope of the present study (cf. e.g. [15]), we want to briefly discuss within the framework of our model, whether fourth-order fluctuations could be measurable or not. Thinking of the higher moments as a probe for the critical point in heavy-ion collision experiments as suggested in [21], it is important to note that, in experiments, a measurement inevitably includes contributions not only from connected diagrams but from all diagrams. For instance, a measured fourth-order fluctuation $\langle AAAA \rangle$ consists not only of the calculated fourth moment $\chi_{aaaa} \equiv \langle AAAA \rangle_c$, but also has contributions from the squared susceptibilities $(\langle AA \rangle_c)^2 = (\chi_{aa})^2$. Hence, the fourth moment is only accessible in experiments if the ratio between the fourth-order fluctuations and the square of their corresponding quadratic fluctuations is larger than the relative error in the measured susceptibilities.

Recalling our definitions for susceptibilities and fourth moments, we find that the ratio of the fluctuations is given by $V\chi_{aaaa}/(\chi_{aa})^2$ with the volume V. As an upper limit, we estimate V to be of the approximate size known for QGPs at freeze-out in heavy-ion collision experiments (e.g. Au-Au collision experiments):

$$V \approx (10\,\mathrm{fm})^3 = 1.30 \cdot 10^{-4}\,\mathrm{MeV}^{-3}. \tag{5.4}$$

As it has been discussed in Sec. 4, the critical point is reflected most prominently in the fluctuations of the u-quark chiral condensate and the quark-number density. Consequently, we investigate the ratios connected to χ_{uuuu}, $\chi_{\mu\mu\mu\mu}$ and $\chi_{uu\mu\mu}$ because we expect to find a clear signature of the critical point there. For the latter fourth moment, we have to take into account that both, $\chi_{uu}\chi_{\mu\mu}$ and $\chi_{u\mu}^2$, contribute to the quadratic fluctuations. Thus, the ratios are given by

$$R_{\mu\mu} \equiv \frac{\chi_{\mu\mu\mu\mu}V}{(\chi_{\mu\mu})^2}, \qquad R_{u\mu} \equiv \frac{3\chi_{uu\mu\mu}V}{\chi_{uu}\chi_{\mu\mu} + 2\chi_{u\mu}^2}, \qquad R_{uu} \equiv \frac{\chi_{uuuu}V}{(\chi_{uu})^2}. \qquad (5.5)$$

We present the results for $g_V = 0$ and $g_V = 0.1g_S$ as contour plots in Fig. 5.3. We observe that $R_{\mu\mu}$ is almost symmetric to the phase transition while $R_{u\mu}$ and R_{uu} are enhanced in the NG phase. Moreover, we find that the negative peak discussed in the last subsection becomes broader but lower in magnitude as one departs from the critical point. Nevertheless, for all evaluated ratios it turns out that the region where the ratios are not small is a very small area around the critical point. From our simple model studies, we conclude that the fourth-order fluctuations are probably no good probes for the investigation of the critical point since the second-order fluctuations may be too strong to allow a measurement of the unique fourth-order contributions. From their definitions, it can be seen that the ratios depend on the volume linearly. Therefore, even a doubled volume would not change the result significantly.

As a side note, it should be noted that, as well as for the third moment, there is a certain area in the phase diagram, where the fourth moment becomes negative. Provided that the fourth moment could be measured, it would offer additional information on the phase diagram in the sense it was suggested for the third moments in [20].

(a) $R_{\mu\mu}$, $g_V = 0$

(b) $R_{\mu\mu}$, $g_V = 0.1g_S$

(c) $R_{u\mu}$, $g_V = 0$

(d) $R_{u\mu}$, $g_V = 0.1g_S$

(e) R_{uu}, $g_V = 0$

(f) R_{uu}, $g_V = 0.1g_S$
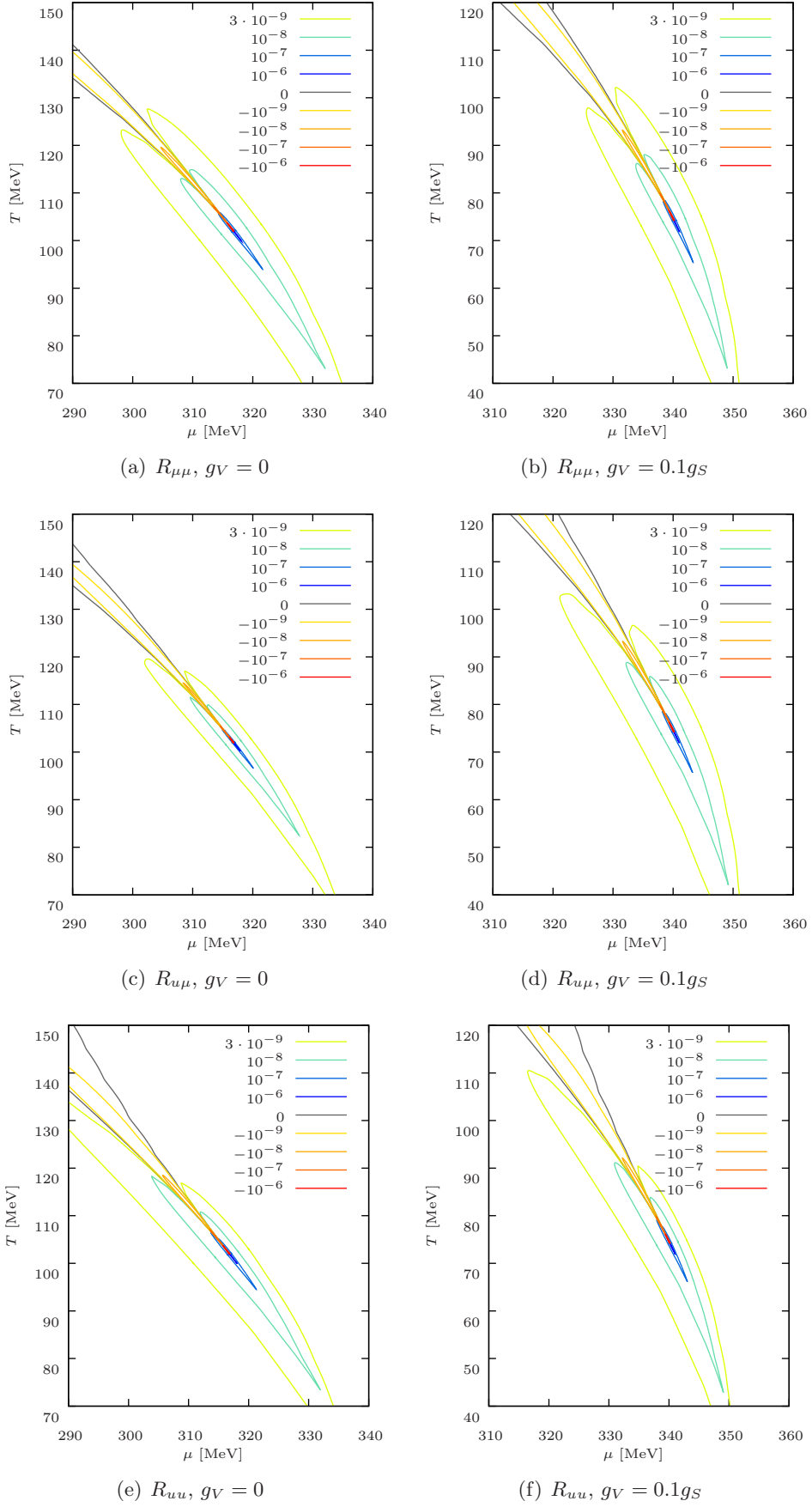
Figure 5.3: The ratios between fourth moments and the squared susceptibilities as defined in (5.5) for $g_V = 0$ and $g_V = 0.1g_S$.

6. Summary and Outlook

Finally, we want to summarize our results and give a brief outlook. In Sec. 2 of the present study, we have reviewed a PNJL model with vector interaction that is almost identical to the one in [7] We have successfully employed this model to investigate susceptibilities in Sec. 4 and third and fourth moments in Sec. 5.

We have determined the critical exponents not only for susceptibilities, but also for the third and fourth moments of the quark-number density. These were found to be in agreement with those suggested in literature [18, 21, 35]. As it has to be expected from universality arguments, the critical exponents are not significantly changed by the vector interaction. Near the CP the magnitude of the susceptibilities, on the other hand, is influenced by the vector interaction. It should be noted that our definition of susceptibilities deviates from the usual definition (cf. [13, 16]) by a factor of T and thus reflects quadratic fluctuations more closely. Although, with the usual definition, the susceptibilities are enhanced in magnitude for increased g_V, we have found that the susceptibilities as we have defined them here - and thus quadratic fluctuations - are rather diminished. This discrepancy is due to the fact that the temperature of the CP is decreased for increased g_V. The vector interaction also affects the critical mode discussed in Sec. 4.1.1. While the main contribution comes from σ_u, the quark-number contribution gains importance as the critical point is approached. For increasing values of g_V, we have observed that the region, where the contributions from the quark-number density are significant, broadens.

As for the calculation of the Ginzburg-Levanyuk criterion for the critical mode, it was not possible to include the Polyakov-loop contribution to the momentum expansion coefficient $\mathfrak{g}$, since our simple model does not allow for such calculations. Based on the finding that the contribution of the Polyakov-loop order parameters to the critical mode are rather small, we have chosen to simply neglect their contributions. Considering (this incomplete) $\mathfrak{g}$, we have found that in a small area the function changes its sign. Although this could be caused by the missing Polyakov-loop contributions, the change of sign may also be present even if all contributions could be considered - meaning that in this area, the preferred phase is inhomogeneous. Such a situation has been found in studies of the NJL model [36]. Evaluating the Ginzburg-Levanyuk criterion, we have again observed that the signature of the critical point is spread over a broader region for increased g_V. Considering the region, where the mean-field approximation is a bad approximation according to the Ginzburg-Levanyuk criterion, we observe that, although this region is larger for $g_V = 0.1g_S$, it is a rather small area for any g_V. It should be noted that we have evaluated the Ginzburg-Levanyuk criterion only in the direction of the critical mode. If, however, the favored phase is inhomogeneous for any condensate, it is hard to imagine that our model could possibly describe the physics properly. Consequently, the region where our mean-field model is insufficient is probably larger than our Ginzburg-Levanyuk criterion suggests. Even if only the Ginzburg-Levanyuk criterion of the critical mode is considered, the critical point and the phase transitions are in the region where the mean-field approximation is judged to be not appropriate. Therefore, instead of the MFA, more sophisticated techniques as a renormalization-group approach [19] would be better choices to describe the physics around the critical point.

In Sec. 5.2, we have checked whether the second-order fluctuations "overshadow" the effect of the fourth-order fluctuations suggested as probes for the CP in [21]. We have found that our model predicts the ratio of the fourth-order fluctuations to the second-order fluctuations to be too small to allow measurements of the fourth-order fluctuations in experiments.

However, the caveats of our PNJL model pointed out in Sec. 2.3 should be acknowledged. As

mentioned above, the MFA is a rather bad approximation in the vicinity of the critical point. This is closely connected to our finding that, around the critical point, an inhomogeneous phase may be favored. Yet, our model is based on the premise of homogeneous matter and it is thus not capable to describe an inhomogenous phase. Moreover, our model only considers chiral condensates $\langle \overline{q}q \rangle$ and the quark-number density $\langle q^\dagger q \rangle$ - but not diquarks. Studies employing the NJL model with diquarks not only suggest the existence of a color-superconducting phase (where $\Delta \neq 0 \wedge \sigma_u \approx 0$)[6], but also the existence of a phase of coexistence (where $\Delta \neq 0 \wedge \sigma_u \neq 0$) [40] and even a BEC phase [41]. These phases are observed in the same region of the phase diagram where the (chiral) first-order phase transition is found. Hence, as g_V is increased, diquarks become more and more important and are likely to strongly influence our findings on the g_V dependence since the critical point is shifted to lower temperatures. Needless to say, that including diquarks into our model would allow for a much improved investigation of the matter. However, this is beyond the scope of this study, because the inclusion of both, the Polyakov-loop and diquarks, in an effective is not an easy task and (to our knowledge) a still unsolved problem [32].

Therefore, improved models which overcome the above mentioned shortcomings of our model are highly desirable in order to investigate fluctuations of second and higher order.

---

[6]Δ denotes the diquark condensate defined in Sec. 2.3.

A. On the Momentum Contribution in the Ginzburg-Lavanyuk Criterion

When calculating expansion coefficient $\mathfrak{g}$ needed for the Ginzburg-Levaniuk criterion, we have to consider the function

$$\left.\frac{\mathrm{d}^2}{\mathrm{d}\vec{q}^2}\Pi_{ab}(0, \vec{q})\right|_{\vec{q}\to 0} \tag{A.1}$$

with the polarization function

$$\Pi_{ab}(iq_4, \vec{q}) = -\int \frac{\mathrm{d}^3 k}{(2\pi)^3} T \sum_n \mathrm{Tr} \frac{1}{\tilde{\slashed{k}} + M}\Gamma_a \frac{1}{\tilde{\slashed{k}} - \slashed{q} + M}\Gamma_b, \tag{A.2}$$

where

$$\tilde{k} = (\vec{k}, k_4 + i\mu), \quad a, b = m_{u,d}, m_s, \mu \quad \text{and} \quad \Gamma_a = \begin{cases} 1 & \text{for } a = m_{u,d}, m_s \\ i\gamma_4 & \text{for } a = \mu \end{cases}. \tag{A.3}$$

This polarization function has been evaluated for the NJL model in [17]. Following the analysis there, it turns out that the results obtained in the NJL model are also applicable in the PNJL model provided that the Fermi-Dirac distribution denoted by $n_\pm$ is replaced with

$$\begin{aligned}
n_+ &= \frac{e^{-3(E-\tilde{\mu})/T} + \bar{\ell}e^{-(E-\tilde{\mu})/T} + 2\ell e^{-2(E-\tilde{\mu})/T}}{1 + e^{-3(E-\tilde{\mu})/T} + 3\bar{\ell}e^{-(E-\tilde{\mu})/T} + 3\ell e^{-2(E-\tilde{\mu})/T}} \\
n_- &= \frac{e^{-3(E+\tilde{\mu})/T} + \ell e^{-(E+\tilde{\mu})/T} + 2\bar{\ell}e^{-2(E+\tilde{\mu})/T}}{1 + e^{-3(E+\tilde{\mu})/T} + 3\ell e^{-(E+\tilde{\mu})/T} + 3\bar{\ell}e^{-2(E+\tilde{\mu})/T}}.
\end{aligned} \tag{A.4}$$

Analogously to [17], we obtain

$$\Pi_{mm}(q_0, \vec{q}) = \nu \int \frac{\mathrm{d}^3 k}{(2\pi)^3} \left(\frac{1 - n_{+1} - n_{-1}}{E_1} + (q^2 - 4M^2)\mathcal{I}(q_0 + i\varepsilon)\right), \tag{A.5a}$$

$$\Pi_{m\mu}(q_0, \vec{q}) = -2M\nu \int \frac{\mathrm{d}^3 k}{(2\pi)^3} \mathcal{I}_\omega(q_0), \tag{A.5b}$$

$$\Pi_{\mu\mu}(q_0, \vec{q}) = \nu \sum_{i=u,d,s} \int \frac{\mathrm{d}^3 k}{(2\pi)^3} \left(\frac{1 - n_{+1} - n_{-1}}{E_1} + (q_0^2 - 4E^2)\mathcal{I}(q_0)\right) \tag{A.5c}$$

with

$$\nu = 2N_c, \quad E = \sqrt{M^2 + \vec{k}^2}, \quad E_{1,2} = \sqrt{M^2 + (\vec{k} \pm \tfrac{1}{2}\vec{q})^2}, \quad n_{\pm 1,2} = n_\pm(E_{1,2}), \tag{A.6}$$

and the frequency sums

$$\begin{aligned}
\mathcal{I}(i\omega) &\equiv T\sum_n \frac{1}{\tilde{k}_4^2 + \vec{k}^2 + M^2}\frac{1}{(\tilde{k}_4 - q_4)^2 + \vec{k}^2 + M^2} \\
&= \frac{-1}{4E_1 E_2}\left(\frac{1 - n_{+1} - n_{-2}}{i\omega - E_1 - E_2} - \frac{n_{-1} - n_{-2}}{i\omega + E_1 - E_2} + \frac{n_{+1} - n_{+2}}{i\omega - E_1 + E_2} - \frac{1 - n_{-1} - n_{+2}}{i\omega + E_1 + E_2}\right)
\end{aligned} \tag{A.7a}$$

36

$$\mathcal{I}_\omega(i\omega) \equiv T \sum_n i(2\tilde{k}_4 - q_4) \frac{1}{\tilde{k}_4^2 + \vec{k}^2 + M^2} \frac{1}{(\tilde{k}_4 - q_4)^2 + \vec{k}^2 + M^2}$$

$$= \frac{1}{4E_2} \left(\frac{1 - n_{+1} - n_{-2}}{i\omega - E_1 - E_2} + \frac{n_{-1} - n_{-2}}{i\omega + E_1 - E_2} + \frac{n_{+1} - n_{+2}}{i\omega - E_1 + E_2} + \frac{1 - n_{-1} - n_{+2}}{i\omega + E_1 + E_2} \right) \tag{A.7b}$$

$$- \frac{1}{4E_1} \left(\frac{1 - n_{+1} - n_{-2}}{i\omega - E_1 - E_2} - \frac{n_{-1} - n_{-2}}{i\omega + E_1 - E_2} - \frac{n_{+1} - n_{+2}}{i\omega - E_1 + E_2} + \frac{1 - n_{-1} - n_{+2}}{i\omega + E_1 + E_2} \right)$$

Differentiating the polarization functions twice and taking the limit $\vec{q} \to 0$, presents us with the result

$$\frac{\mathrm{d}^2}{\mathrm{d}\vec{q}^2} \Pi_{mm}(0, \vec{q}) \Big|_{\vec{q} \to 0} = \nu \int \frac{\mathrm{d}^3 k}{(2\pi)^3} \left(\left(-\frac{\mathrm{d}^2 n_+}{\mathrm{d}E^2} - \frac{\mathrm{d}^2 n_-}{\mathrm{d}E^2} + 3\frac{\frac{\mathrm{d}n_+}{\mathrm{d}E} + \frac{\mathrm{d}n_-}{\mathrm{d}E}}{E} + 3\frac{1 - n_- - n_+}{E^2} \right) \frac{k^2}{4E^3} \right.$$

$$+ \left(-\frac{\mathrm{d}n_-}{\mathrm{d}E} - \frac{\mathrm{d}n_+}{\mathrm{d}E} - \frac{1 - n_- - n_+}{E} \right) \frac{1}{4E^2}$$

$$\left. -4M^2 \frac{\mathrm{d}^2 \mathcal{I}(0)}{\mathrm{d}\vec{q}^2} \Big|_{\vec{q}=0} - 2\, \mathcal{I}(0)|_{\vec{q}=0} \right), \tag{A.8a}$$

$$\frac{\mathrm{d}^2}{\mathrm{d}\vec{q}^2} \Pi_{m\mu}(0, \vec{q}) \Big|_{\vec{q} \to 0} = -2M\nu \int \frac{\mathrm{d}^3 k}{(2\pi)^3} \frac{\mathrm{d}^2 \mathcal{I}_\omega(0)}{\mathrm{d}\vec{q}^2} \Big|_{\vec{q}=0}, \tag{A.8b}$$

$$\frac{\mathrm{d}^2}{\mathrm{d}\vec{q}^2} \Pi_{\mu\mu}(0, \vec{q}) \Big|_{\vec{q} \to 0} = \nu \sum_{i=u,d,s} \int \frac{\mathrm{d}^3 k}{(2\pi)^3} \left(\left(-\frac{\mathrm{d}^2 n_+}{\mathrm{d}E^2} - \frac{\mathrm{d}^2 n_-}{\mathrm{d}E^2} + 3\frac{\frac{\mathrm{d}n_+}{\mathrm{d}E} + \frac{\mathrm{d}n_-}{\mathrm{d}E}}{E} + 3\frac{1 - n_- - n_+}{E^2} \right) \frac{k^2}{4E^3} \right.$$

$$\left. + \left(-\frac{\mathrm{d}n_-}{\mathrm{d}E} - \frac{\mathrm{d}n_+}{\mathrm{d}E} - \frac{1 - n_- - n_+}{E} \right) \frac{1}{4E^2} - 4E^2 \frac{\mathrm{d}^2 \mathcal{I}(0)}{\mathrm{d}\vec{q}^2} \Big|_{\vec{q}=0} \right), \tag{A.8c}$$

with

$$\mathcal{I}(0)|_{\vec{q}=0} = \frac{1}{4E^2} \left(\frac{1 - n_+ - n_-}{E} + \frac{\mathrm{d}n_+}{\mathrm{d}E} + \frac{\mathrm{d}n_-}{\mathrm{d}E} \right), \tag{A.9a}$$

$$\frac{\mathrm{d}^2 \mathcal{I}(0)}{\mathrm{d}\vec{q}^2} \Big|_{\vec{q}=0} = \left(-\frac{1 - n_+ - n_-}{E} - \frac{\mathrm{d}n_+}{\mathrm{d}E} - \frac{\mathrm{d}n_-}{\mathrm{d}E} \right) \left(-\frac{1}{2E^4} \left(\frac{\vec{k}}{2E} \right)^2 + \frac{3}{4E^3} \frac{M^2}{4E^3} \right)$$

$$+ \frac{1}{3E^2} \left(\frac{\mathrm{d}^3 n_-}{\mathrm{d}E^3} + \frac{\mathrm{d}^3 n_+}{\mathrm{d}E^3} \right) \left(\frac{\vec{k}}{2E} \right)^2, \tag{A.9b}$$

$$\frac{\mathrm{d}^2 \mathcal{I}_\omega(0)}{\mathrm{d}\vec{q}^2} \Big|_{\vec{q}=0} = \frac{1}{2E^3} \left(\frac{\mathrm{d}n_-}{\mathrm{d}E} - \frac{\mathrm{d}n_+}{\mathrm{d}E} \right) \left(\left(\frac{\vec{k}}{2E} \right)^2 - \frac{M^2}{4E^2} \right) + \frac{1}{E^2} \left(\frac{\mathrm{d}^2 n_-}{\mathrm{d}E^2} - \frac{\mathrm{d}^2 n_+}{\mathrm{d}E^2} \right) \left(\frac{\vec{k}}{2E} \right)^2$$

$$+ \frac{2}{3E} \left(\frac{\mathrm{d}^3 n_-}{\mathrm{d}E^3} - \frac{\mathrm{d}^3 n_+}{\mathrm{d}E^3} \right) \left(\frac{\vec{k}}{2E} \right)^2. \tag{A.9c}$$

In the above calculation, we have excessively used that, in the limit of $\vec{q} \to 0$,

$$E_2 = E_1, \quad -\frac{\mathrm{d}E_2}{\mathrm{d}q} = \frac{\mathrm{d}E_1}{\mathrm{d}q} = \frac{\vec{k}}{2E}, \quad \text{and} \quad \frac{\mathrm{d}^2 E_2}{\mathrm{d}q^2} = \frac{\mathrm{d}^2 E_1}{\mathrm{d}q^2} = \frac{M^2}{4E^3}. \tag{A.10}$$

B. On the Calculation of Third and Fourth Moments

In this section, we describe how the third and fourth moment are calculated in detail. At first, let us introduce a simplified notation. We will write derivatives with respect to mass-like terms by appending an index a,b,c,d and derivatives with respect to condensates by appending an index i,j,k,l to the quantity. For example, we have

$$\Omega_{ai} \equiv \frac{\partial^2 (\Omega/(VT))}{\partial \mathfrak{m}_a \partial \langle \rangle_i}, \qquad \langle \rangle_{j,a} \equiv \frac{\mathrm{d} \langle \rangle_j}{\mathrm{d} \mathfrak{m}_a}. \tag{B.1}$$

Note that we separate the indices originating from differentiation from other indices with a comma. With this notation, the third moment

$$\frac{\mathrm{d}^3 (\Omega/(VT))}{\mathrm{d} \mathfrak{m}_a \mathrm{d} \mathfrak{m}_b \mathrm{d} \mathfrak{m}_c} = \Omega_{abc} + \sum_j \Omega_{abj} \langle \rangle_{j,c} + \sum_j \Omega_{ajc} \langle \rangle_{j,b} + \sum_{j,k} \Omega_{ajk} \langle \rangle_{j,b} \langle \rangle_{k,c} + \sum_j \Omega_{aj} \langle \rangle_{j,bc} \tag{B.2}$$

is found by differentiating (4.4). In (B.2), $\langle \rangle_{j,c}$ is already known from the calculation of the susceptibilities as the solution of (4.5). Analogously, differentiating the gap equations twice yields

$$\sum_j \Omega_{ij} \langle \rangle_{j,bc} = - \left(\Omega_{ibc} + \sum_j \Omega_{ibj} \langle \rangle_{j,c} + \sum_j \Omega_{ijc} \langle \rangle_{j,b} + \sum_{j,k} \Omega_{ijk} \langle \rangle_{j,b} \langle \rangle_{k,c} \right). \tag{B.3}$$

Since all quantities on the right side are known, this provides us with a system of linear equations which can be solved for $\langle \rangle_{j,bc}$. As for the fourth moments, we proceed in the same way. We derive (B.2) once again to obtain

$$\begin{aligned}
\frac{\mathrm{d}^4 (\Omega/(VT))}{\mathrm{d} \mathfrak{m}_a \mathrm{d} \mathfrak{m}_b \mathrm{d} \mathfrak{m}_c \mathrm{d} \mathfrak{m}_d} =& \Omega_{abcd} + \sum_j \left(\left[\Omega_{abcj} \langle \rangle_{j,d} + \sum_k \Omega_{abjk} \langle \rangle_{j,c} \langle \rangle_{k,d} + \Omega_{abj} \langle \rangle_{j,cd} + \sum_k \Omega_{ajk} \langle \rangle_{j,bc} \langle \rangle_{k,d} \right] \right. \\
& \left. + \text{cyclic permutations of } [\,] \text{ with respect to } b, c, d \right) \\
& + \sum_{j,k,l} \Omega_{ajkl} \langle \rangle_{j,b} \langle \rangle_{k,c} \langle \rangle_{l,d} + \sum_j \Omega_{aj} \langle \rangle_{j,bcd}.
\end{aligned} \tag{B.4}$$

$\langle \rangle_{j,bcd}$ is achieved by solving

$$\begin{aligned}
\sum_j \Omega_{ij} \langle \rangle_{j,bcd} =& - \left(\Omega_{ibcd} + \sum_j \left(\left[\Omega_{ijbc} \langle \rangle_{j,d} + \sum_k \Omega_{ijkb} \langle \rangle_{j,c} \langle \rangle_{k,d} + \Omega_{ijb} \langle \rangle_{j,cd} + \sum_k \Omega_{ijk} \langle \rangle_{j,bc} \langle \rangle_{k,d} \right] \right.\right. \\
& \left. + \text{cyclic permutations of } [\,] \text{ with respect to } b, c, d \right) \\
& \left. + \sum_{j,k,l} \Omega_{ijkl} \langle \rangle_{j,b} \langle \rangle_{k,c} \langle \rangle_{l,d} \right),
\end{aligned} \tag{B.5}$$

where the solutions of (4.5) and (B.4) have to be employed to determine the right side.

References

[1] D. J. Gross and F. Wilczek, Phys. Rev. Lett. **30** (1973) 1343;
H. D. Politzer, Phys. Rev. Lett. **30**, 1346 (1973).

[2] Y. Nambu and G. Jona-Lasinio, Phys. Rev. **122** (1961) 345;
Y. Nambu and G. Jona-Lasinio, Phys. Rev. **124** (1961) 246.

[3] T. Hatsuda and T. Kunihiro, Phys. Rept. **247** (1994) 221.

[4] S. P. Klevansky, Rev. Mod. Phys. **64** (1992) 649.

[5] M. Buballa, Phys. Rept. **407** (2005) 205.

[6] K. Fukushima, Phys. Lett. B **591** (2004) 277.

[7] K. Fukushima, Phys. Rev. D **77** (2008) 114028 [Erratum-ibid. D **78** (2008) 039902].

[8] C. Ratti, M. A. Thaler and W. Weise, Phys. Rev. D **73** (2006) 014019.

[9] S. Roessner, C. Ratti and W. Weise, Phys. Rev. D **75** (2007) 034007.

[10] P. Braun-Munzinger and J. Wambach, Rev. Mod. Phys. **81**, (2009) 1031.

[11] M. G. Alford, A. Schmitt, K. Rajagopal and T. Schafer, Rev. Mod. Phys. **80** (2008) 1455.

[12] N. Yamamoto, M. Tachibana, T. Hatsuda and G. Baym, Phys. Rev. D **76** (2007) 074001.

[13] L. D. Landau and E. M. Lifshitz, *Statistical Physics, Third Edition, Part 1* (Butterworth-Heinemann, 1980).

[14] M. A. Stephanov, K. Rajagopal and E. V. Shuryak, Phys. Rev. Lett. **81** (1998) 4816.

[15] M. A. Stephanov, K. Rajagopal and E. V. Shuryak, Phys. Rev. D **60** (1999) 114028.

[16] T. Kunihiro, Phys. Lett. B **271** (1991) 395.

[17] H. Fujii and M. Ohtani, Phys. Rev. D **70** (2004) 014016.

[18] Y. Hatta and T. Ikeda, Phys. Rev. D **67** (2003) 014028.

[19] B. J. Schaefer and J. Wambach, Phys. Rev. D **75** (2007) 085015.

[20] M. Asakawa, S. Ejiri and M. Kitazawa, Phys. Rev. Lett. **103** (2009) 262301.

[21] M. A. Stephanov, Phys. Rev. Lett. **102**, 032301 (2009).

[22] M. E. Peskin and D. V. Schroeder, *An Introduction to Quantum Field Theory* (Perseus Books, 1995).

[23] J. I. Kapusta and C. Gale, *Finite-Temperature Field Theory: Principles and Applications* (Cambridge University Press, 2006).

[24] K. Yagi, T. Hatsuda and Y. Miake, *Quark-Gluon Plasma: From Big Bang To Little Bang*, (Camb. Monogr. Part. Phys. Nucl. Phys. Cosmol. **23**, 2005).

[25] K. G. Wilson, Phys. Rev. D **10** (1974) 2445.

[26] M. A. Stephanov, PoS **LAT2006** (2006) 024 [arXiv:hep-lat/0701002].

[27] M. Kobayashi and T. Maskawa, Prog. Theor. Phys. **44** (1970) 1422;
M. Kobayashi, H. Kondo and T. Maskawa, Prog. Theor. Phys. **45** (1971) 1955.

[28] C. Amsler et al. (Particle Data Group), PL **B667**, 1 (2008) and 2009 partial update for the 2010 edition (`http://pdg.lbl.gov`).

[29] R. Rapp, T. Schäfer, E. V. Shuryak and M. Velkovsky, Phys. Rev. Lett. **81** (1998) 53.

[30] A. M. Polyakov, Nucl. Phys. B **120** (1977) 429;
L. Susskind, Phys. Rev. D **20** (1979) 2610.

[31] K. Fukushima, Annals Phys. **304** (2003) 72.

[32] H. Abuki and K. Fukushima, Phys. Lett. B **676**, 57 (2009).

[33] L. McLerran, K. Redlich and C. Sasaki, Nucl. Phys. A **824** (2009) 86.

[34] L. McLerran and R. D. Pisarski, Nucl. Phys. A **796** (2007) 83;
Y. Hidaka, L. D. McLerran and R. D. Pisarski, Nucl. Phys. A **808** (2008) 117.

[35] R. B. Griffiths and J. C. Wheeler, Phys. Rev. A **2** (1970) 1047.

[36] D. Nickel, Phys. Rev. D **80** (2009) 074025.

[37] S. Carignano, D. Nickel and M. Buballa, arXiv:1007.1397v1 [hep-ph].

[38] B. Stokic, B. Friman and K. Redlich, Phys. Lett. B **673**, 192 (2009).

[39] see, for example: `http://www.autodiff.org/`;
`https://projects.coin-or.org/ADOL-C/browser/stable/2.1/ADOL-C/doc/adolc-manual.pdf`;
M. Wagner, PhD Thesis (2009), `http://tuprints.ulb.tu-darmstadt.de/1317/`.

[40] M. Kitazawa, T. Koide, T. Kunihiro and Y. Nemoto, Prog. Theor. Phys. **108**, 929 (2002).

[41] H. Abuki, G. Baym, T. Hatsuda and N. Yamamoto, Phys. Rev. D **81**, 125010 (2010).